JHEP

Published for SISSA by Springer

Received: March 9, 2022
Accepted: April 16, 2022
Published: May 17, 2022

Probing light mediators and $(g-2)_\mu$ through detection of coherent elastic neutrino nucleus scattering at COHERENT

M. Atzori Corona,[a,b] **M. Cadeddu,**[b] **N. Cargioli,**[a,b] **F. Dordei,**[b] **C. Giunti,**[c] **Y.F. Li,**[d,e] **E. Picciau,**[a,b] **C.A. Ternes**[c] **and Y.Y. Zhang**[d,e,1]

[a] *Dipartimento di Fisica, Università degli Studi di Cagliari, Complesso Universitario di Monserrato — S.P. per Sestu Km 0.700, 09042 Monserrato (Cagliari), Italy*

[b] *Istituto Nazionale di Fisica Nucleare (INFN), Sezione di Cagliari, Complesso Universitario di Monserrato — S.P. per Sestu Km 0.700, 09042 Monserrato (Cagliari), Italy*

[c] *Istituto Nazionale di Fisica Nucleare (INFN), Sezione di Torino, Via P. Giuria 1, I-10125 Torino, Italy*

[d] *Institute of High Energy Physics, Chinese Academy of Sciences, Beijing 100049, China*

[e] *School of Physical Sciences, University of Chinese Academy of Sciences, Beijing 100049, China*

E-mail: mattia.atzori.corona@ca.infn.it, matteo.cadeddu@ca.infn.it, nicola.cargioli@ca.infn.it, francesca.dordei@cern.ch, carlo.giunti@to.infn.it, liyufeng@ihep.ac.cn, emmanuele.picciau@ca.infn.it, ternes@to.infn.it, zhangyiyu@ihep.ac.cn

Abstract: We present the constraints on the parameters of several light boson mediator models obtained from the analysis of the current data of the COHERENT CEνNS experiment. We consider a variety of vector boson mediator models: the so-called universal, the $B-L$ and other anomaly-free U(1)$'$ gauge models with direct couplings of the new vector boson with neutrinos and quarks, and the anomaly-free L_e-L_μ, L_e-L_τ, and $L_\mu-L_\tau$ gauge models where the coupling of the new vector boson with the quarks is generated by kinetic mixing with the photon at the one-loop level. We consider also a model with a new light scalar boson mediator that is assumed, for simplicity, to have universal coupling with quarks and leptons. Since the COHERENT CEνNS data are well-fitted with the cross section predicted by the Standard Model, the analysis of the data yields constraints for the mass and coupling of the new boson mediator that depend on the charges of quarks and neutrinos in each model under consideration. We compare these constraints with the limits obtained in other experiments and with the values that can explain the muon $g-2$ anomaly in the models where the muon couples to the new boson mediator.

Keywords: Neutrino Interactions, New Light Particles

ArXiv ePrint: 2202.11002

[1] Corresponding author.

https://doi.org/10.1007/JHEP05(2022)109

Contents

1 Introduction **1**

2 COHERENT data analysis **3**

3 CEνNS process and light mediators **6**
- 3.1 Light vector mediator 7
- 3.2 Light scalar mediator 14

4 Constraints on light mediator models **16**
- 4.1 Universal Z' model 17
- 4.2 $B - L$ model 19
- 4.3 $B_y + L_\mu + L_\tau$ model 20
- 4.4 $B - 3L_e$ model 21
- 4.5 $B - 3L_\mu$ model 21
- 4.6 $B - 2L_e - L_\mu$ model 21
- 4.7 $B - L_e - 2L_\mu$ model 23
- 4.8 $L_e - L_\mu$ model 23
- 4.9 $L_e - L_\tau$ model 23
- 4.10 $L_\mu - L_\tau$ model 25
- 4.11 Scalar model 25

5 Conclusions **26**

A Z' coupling **27**

B Muon $g - 2$ **28**

JHEP05(2022)109

1 Introduction

The discovery of coherent elastic neutrino-nucleus scattering (CEνNS) in cesium-iodide (CsI) by the COHERENT Collaboration [1, 2] sparked a flood of research into a variety of physical processes, with substantial implications for particle physics, astrophysics, nuclear physics, and beyond [3–10, 10–20]. After the discovery in 2017 of CEνNS with the CsI detector, the COHERENT Collaboration accomplished in 2020 the first observation of CEνNS in argon (Ar) [21, 22] and updated in 2021 the results obtained with the CsI detector [23]. By combining the greater CEνNS statistics with a refined quenching factor estimation for the CsI measurement and by virtue of the complementary role of two different target nuclei, more stringent tests of nuclear physics, neutrino properties, electroweak interactions, and new physics beyond the Standard Model (SM) have been performed [24–28].

The CEνNS process happens when the momentum transfer between the incoming neutrino and the target nucleus is so small that the wavelength of the boson which mediates the interaction is larger than the nuclear radius, so that the neutrino interacts with the nucleus as a whole and the cross section is proportional to the square of the number of nucleons participating to the process. The CEνNS process is a pure neutral current interaction which is mediated by the exchange of the Z vector boson in the SM, but it can also receive contributions from other hypothetical neutral bosons in theories beyond the SM. Therefore, it turns out to be a powerful tool to probe new physics interactions beyond the SM [5–10].

In this paper we test new physics models with interactions mediated by a light vector or scalar boson that contribute to the CEνNS process by analyzing the recently released 2021 CsI data [23] and the 2020 Ar data [21, 22] of the COHERENT experiment. For each model, we present the constraints on the mass and coupling of the light vector or scalar boson mediator that we obtained from the separate and combined fits of the CsI and Ar COHERENT CEνNS data. Comparing with the previous publication in ref. [26], we have considered a larger variety of vector mediator models, we have included the scalar mediator model, and we have updated the analysis using the recently released 2021 CsI data [23].

We also consider the possible explanation of the 4.2σ difference between the SM prediction [29–54] of the value of the muon anomalous magnetic moment $(g-2)_\mu$ and the combination of the values measured at the Brookhaven National Laboratory [55] and recently at the Fermi National Laboratory [56]. This so-called $(g-2)_\mu$ anomaly is a putative signal of physics beyond the SM, which has been studied in many papers (see, e.g., refs. [57, 58]). Interestingly, several light vector mediator models are regarded as candidate solutions (see, e.g., refs. [59–67]), but also a light scalar mediator have the potential to solve the anomaly [68]. Among the models that we consider in this paper, those in which the muon interacts with the new light boson mediator can explain the $(g-2)_\mu$ anomaly. For these models, we compare the constraints on the mass and coupling of the new light boson mediator obtained from the analysis of the COHERENT CEνNS data and those obtained by other experiments focusing on the parameter region that can solve the $(g-2)_\mu$ anomaly. There are many studies of extensions of the SM with the addition of a U(1)$'$ gauge group with an associated neutral vector gauge boson Z' (see, e.g., the review in ref. [69]). The models differ in the charges of the fermions, which determine the contributions to CEνNS of the interactions mediated by the Z' vector boson. These contributions add coherently to the SM weak neutral current interactions which are mediated by the Z vector boson. The effects are quantified by additional terms in the weak charge of the nucleus. Note that the effects on the CEνNS process of the interactions mediated by a light boson are different from those induced by the so-called non-standard interactions (NSI), that arise in an effective four-fermion theory in which the heavy mediator has been integrated out. In the case of NSI there is a global rescaling of the CEνNS cross section that depends on the interaction parameters of the NSI, whereas a light boson mediator can alter the nuclear recoil energy spectrum through the boson propagator that depends on the momentum transfer. This effect generates distinct spectral features that can be probed with the experimental observations.

In this paper we first consider the so-called universal Z' model in which all the standard fermions have the same charge [6, 12, 14, 15, 26, 70, 71]. This model is not anomaly-free per

JHEP05(2022)109

se, but it can be extended with new non-standard particles to make it anomaly-free. Then, we consider several U(1)$'$ models in which quarks and leptons have appropriate non-zero charges that cancel the quantum anomalies (e.g., the popular $B-L$ model [69, 72, 73], where B is the baryon number and L is the total lepton number). Since in these models the Z' vector boson interacts directly with neutrinos and nucleons, the CEνNS process occurs at tree level and it is possible to obtain stringent constraints on the mass and coupling of the new vector boson from the COHERENT CEνNS data.

We also consider the anomaly-free $L_e - L_\mu$, $L_e - L_\tau$, and $L_\mu - L_\tau$ U(1)$'$ models [74–77] (where L_α are the lepton generation numbers, for $\alpha = e, \mu, \tau$) in which the charges are exclusively leptonic. However, in these models there are contributions to the CEνNS process, which occur through the kinetic mixing of the Z' boson with the photon, that is generated at one-loop level [28, 78, 79], and the interaction of the photon with the protons in the target nuclei. Therefore, we can constrain the mass and coupling of the vector boson in these models using the COHERENT CEνNS data, albeit less tightly than in the models with direct quark-Z' interactions, because of the weaker one-loop interaction.

We consider also contributions to the CEνNS process of interactions mediated by a light scalar boson [7, 10, 80–82], which differ from those mediated by a light vector boson for the following two fundamental reasons. First, the helicity-flipping interactions mediated by a scalar boson contribute incoherently to the CEνNS process with respect to the helicity-conserving SM contribution, contrary to the helicity-conserving interactions mediated by a new vector boson that contribute coherently. Therefore, in the scalar case, the new contribution consists in an addition to the cross section, not to the amplitude of the process as in the vector case. Second, the scalar charges of the nucleons are not simply given by the sum of the charges of the valence quarks as in the vector case, because the scalar currents are not conserved as the vector currents. Therefore, the scalar charges of the nucleons must be calculated and the results have large theoretical uncertainties.

The paper is organized as follows. In section 2 the method of the COHERENT data analysis is described. In section 3, we present the cross section of the CEνNS process and summarize the models of light mediators and the corresponding effects on the CEνNS cross section. In section 4, the COHERENT CEνNS constraints on the allowed parameter space of the light mediator models are presented and compared with the $(g-2)_\mu$ allowed regions and other current limits. Finally, we conclude and summarize our results in section 5.

2 COHERENT data analysis

The CEνNS event energy spectra in the COHERENT experiment depend on the neutrino flux produced by the pion decay. The total differential neutrino flux is given by the sum of the three neutrino components, where the first prompt component is coming from the pion decay ($\pi^+ \to \mu^+ + \nu_\mu$), and the second two delayed components are coming from the

JHEP05(2022)109

subsequent muon decay ($\mu^+ \to e^+ + \nu_e + \bar{\nu}_\mu$)

$$\frac{dN_{\nu_\mu}}{dE} = \eta\,\delta\left(E - \frac{m_\pi^2 - m_\mu^2}{2m_\pi}\right), \tag{2.1}$$

$$\frac{dN_{\nu_{\bar{\mu}}}}{dE} = \eta\,\frac{64E^2}{m_\mu^3}\left(\frac{3}{4} - \frac{E}{m_\mu}\right), \tag{2.2}$$

$$\frac{dN_{\nu_e}}{dE} = \eta\,\frac{192E^2}{m_\mu^3}\left(\frac{1}{2} - \frac{E}{m_\mu}\right). \tag{2.3}$$

Here, E is the neutrino energy, m_π and m_μ are the pion and muon masses, and $\eta = rN_{\rm POT}/4\pi L^2$ is the normalization factor, where r is the number of neutrinos per flavor produced for each proton-on-target (POT), $N_{\rm POT}$ is the number of POT, and L is the baseline between the source and the detector. For the COHERENT Ar detector, called CENNS-10, we use $r = 0.09$, $N_{\rm POT} = 13.7\cdot10^{22}$ and $L = 27.5$ m [22]. For the COHERENT CsI detector, we use $r = 0.0848$, $N_{\rm POT} = 3.198\cdot10^{23}$ and $L = 19.3$ m [23].

The theoretical CEνNS event number $N_i^{\rm CE\nu NS}$ in each nuclear-recoil energy-bin i is given by

$$N_i^{\rm CE\nu NS} = N(\mathcal{N})\int_{T_{\rm nr}^i}^{T_{\rm nr}^{i+1}} dT_{\rm nr} A(T_{\rm nr}) \int_0^{T'^{\rm max}_{\rm nr}} dT'_{\rm nr} R(T_{\rm nr}, T'_{\rm nr}) \int_{E_{\rm min}(T'_{\rm nr})}^{E_{\rm max}} dE \sum_{\nu=\nu_e,\nu_\mu,\bar{\nu}_\mu} \frac{dN_\nu}{dE}(E)\frac{d\sigma_{\nu-\mathcal{N}}}{dT_{\rm nr}}(E, T'_{\rm nr}), \tag{2.4}$$

where $T_{\rm nr}$ is the reconstructed nuclear recoil kinetic energy, $T'_{\rm nr}$ is the true nuclear recoil kinetic energy, $A(T_{\rm nr})$ is the energy-dependent detector efficiency, $R(T_{\rm nr}, T'_{\rm nr})$ is the energy resolution function, $T'^{\rm max}_{\rm nr} = 2E^2_{\rm max}/M$, $E_{\rm max} = m_\mu/2 \sim 52.8\,{\rm MeV}$, $E_{\rm min}(T'_{\rm nr}) = \sqrt{MT'_{\rm nr}/2}$, m_μ being the muon mass, M the nuclear mass, and $N(\mathcal{N})$ the number of $\mathcal{N}$ atoms in the detector. We obtained information on these quantities from refs. [21, 22] for the Ar data and from ref. [23] for the CsI data. The number of $\mathcal{N}$ atoms in each detector is given by $N(\mathcal{N}) = N_{\rm A}M_{\rm det}/M_{\mathcal{N}}$, where $N_{\rm A}$ is the Avogadro number, $M_{\rm det}$ is the detector active mass ($M_{\rm det} = 24$ kg for Ar and $M_{\rm det} = 14.6$ kg for CsI), and $M_{\mathcal{N}}$ is the molar mass ($M_{\rm Ar} = 39.96$ g/mol and $M_{\rm CsI} = 259.8$ g/mol). The differential CEνNS cross section $d\sigma_{\nu-\mathcal{N}}/dT_{\rm nr}$ is discussed in section 3.

Due to the quenching effect, the energy actually observed is the electron-equivalent recoil energy T_{ee}, which is transformed into the nuclear recoil energy $T_{\rm nr}$ by inverting the relation

$$T_{ee} = f_Q\,(T_{\rm nr})\,T_{\rm nr}, \tag{2.5}$$

where f_Q is the quenching factor, which is given in refs. [23, 83] for the CsI detector and in ref. [22] for the Ar detector.

An important characteristic of the neutrino beam in the COHERENT experiment is the time dependence of the neutrino flavor components: the prompt ν_μ's produced in fast pion decay ($\tau_{\pi^\pm} \simeq 26$ ns) arrive within about 1 μs from the on-beam trigger, whereas the delayed ν_e's and $\bar{\nu}_\mu$'s produced in the slower muon decay ($\tau_{\mu^\pm} \simeq 2.2$ μs) arrive in a time interval which tails out at about 10 μs. Therefore, taking into account the time evolution of the data is useful for distinguishing the interactions of the two neutrino flavors. We implemented

JHEP05(2022)109

the analyses of the COHERENT CsI and Ar data using the timing information provided by the COHERENT Collaboration [22, 23, 83] and distributing the theoretical CEνNS event numbers $N_i^{\mathrm{CE}\nu\mathrm{NS}}$ in eq. (2.4) in time bins that are calculated from the exponential decay laws of the generating pions and muons. With this procedure we obtained the theoretical CEνNS event numbers $N_{ij}^{\mathrm{CE}\nu\mathrm{NS}}$, where i is the index of the energy bins and j is the index of the time bins.

We performed the analysis of the COHERENT CsI data in the energy and time bins considered in ref. [23]. Since in some energy-time bins the number of events is zero, we used the Poissonian least-squares function [84, 85]

$$\chi^2_{\mathrm{CsI}} = 2\sum_{i=1}^{9}\sum_{j=1}^{11}\left[\sum_{z=1}^{4}(1+\eta_z)N_{ij}^z - N_{ij}^{\mathrm{exp}} + N_{ij}^{\mathrm{exp}}\ln\left(\frac{N_{ij}^{\mathrm{exp}}}{\sum_{z=1}^{4}(1+\eta_z)N_{ij}^z}\right)\right] + \sum_{z=1}^{4}\left(\frac{\eta_z}{\sigma_z}\right)^2, \tag{2.6}$$

where the indices i and j denote, respectively, the energy and time bins, and the indices $z = 1, 2, 3, 4$ stand for CEνNS, beam-related neutron (BRN), neutrino-induced neutron (NIN), and steady-state (SS) backgrounds, respectively. In our notation, N_{ij}^{exp} is the experimental event number obtained from coincidence (C) data, $N_{ij}^{\mathrm{CE}\nu\mathrm{NS}}$ is the predicted number of CEνNS events that depends on the physics model under consideration, N_{ij}^{BRN} is the estimated BRN background, N_{ij}^{NIN} is the estimated NIN background, and N_{ij}^{SS} is the SS background obtained from the anti-coincidence (AC) data. We took into account the systematic uncertainties described in ref. [23] with the nuisance parameters η_z and the corresponding uncertainties $\sigma_{\mathrm{CE}\nu\mathrm{NS}} = 0.12$ (which is the systematic uncertainty of the signal rate considering the effects of the 10%, 3.8%, 4.1%, and 3.4% uncertainties of the neutrino flux, quenching factor, CEνNS efficiency, and neutron form factors, respectively), $\sigma_{\mathrm{BRN}} = 0.25$, $\sigma_{\mathrm{NIN}} = 0.35$, and $\sigma_{\mathrm{SS}} = 0.021$.

We performed the analysis of the COHERENT Ar data in the energy and time bins given in the data release [22] with the least-squares function

$$\chi^2_{\mathrm{Ar}} = \sum_{i=1}^{12}\sum_{j=1}^{10}\left(\frac{N_{ij}^{\mathrm{exp}} - \sum_{z=1}^{4}(1+\eta_z+\sum_l \eta_{zl,ij}^{\mathrm{sys}})N_{ij}^z}{\sigma_{ij}}\right)^2 + \sum_{z=1}^{4}\left(\frac{\eta_z}{\sigma_z}\right)^2 + \sum_{z,l}(\epsilon_{zl})^2\,, \tag{2.7}$$

where i is the index of the energy bins and j is the index of the time bins. Here $z = 1, 2, 3, 4$ stands for the theoretical prediction of CEνNS, Steady-State (SS), Prompt Beam-Related Neutron (PBRN) and Delayed Beam-Related Neutron (DBRN) backgrounds, and N_{ij}^{exp} is the number of observed events in each energy and time bin. The statistical uncertainty σ_{ij} is given by

$$(\sigma_{ij})^2 = (\sigma_{ij}^{\mathrm{exp}})^2 + (\sigma_{ij}^{\mathrm{SS}})^2, \tag{2.8}$$

where $\sigma_{ij}^{\mathrm{exp}} = \sqrt{N_{ij}^{\mathrm{exp}}}$ and $\sigma_{ij}^{\mathrm{SS}} = \sqrt{N_{ij}^{\mathrm{SS}}/5}$. The factor 1/5 is due to the 5 times longer sampling time of the SS background with respect to the signal time window. The nuisance parameters η_z quantify the systematic uncertainties of the event rate for the theoretical prediction of CEνNS, SS, PBRN, and DBRN backgrounds, with the corresponding uncertainties $\sigma_{\mathrm{CE}\nu\mathrm{NS}} = 0.13$, $\sigma_{\mathrm{PBRN}} = 0.32$, $\sigma_{\mathrm{DBRN}} = 1$, and $\sigma_{\mathrm{SS}} = 0.0079$. We considered also the systematic uncertainties of the shapes of CEνNS and PBRN spectra using the

JHEP05(2022)109

information in the COHERENT data release [22]. This is done in eq. (2.7) through the nuisance parameters ϵ_{zl} and the terms $\eta^{\rm sys}_{zl,ij}$ given by

$$\eta^{\rm sys}_{zl,ij} = \epsilon_{zl}\,\frac{N^{\rm sys}_{zl,ij} - N^{\rm CV}_{zl,ij}}{N^{\rm CV}_{zl,ij}}, \tag{2.9}$$

where l is the index of the source of the systematic uncertainty. Here $N^{\rm sys}_{zl,ij}$ and $N^{\rm CV}_{zl,ij}$ are, respectively, 1σ probability distribution functions (PDFs) described in table 3 of ref. [22] and the central-value (CV) SM predictions described in table 2 of ref. [22]. For the theoretical prediction of CEνNS ($z = 1$), the sources of systematic shape uncertainties are the F_{90} energy dependence and the mean time to trigger ($t_{\rm trig}$) distribution. For the PBRN background ($z = 2$), the sources of systematic shape uncertainties are the energy, $t_{\rm trig}$ mean, and $t_{\rm trig}$ width distributions.

3 CEνNS process and light mediators

In the SM, the differential cross section as a function of the nuclear kinetic recoil energy $T_{\rm nr}$ of the CEνNS process with a neutrino ν_ℓ ($\ell = e, \mu, \tau$) and a nucleus $\mathcal{N}$ is given by [86–88]

$$\frac{d\sigma_{\nu_\ell\text{-}\mathcal{N}}}{dT_{\rm nr}}(E, T_{\rm nr}) = \frac{G_{\rm F}^2 M}{\pi}\left(1 - \frac{MT_{\rm nr}}{2E^2}\right)(Q^V_{\ell,\rm SM})^2, \tag{3.1}$$

where $G_{\rm F}$ is the Fermi constant and

$$Q^V_{\ell,\rm SM} = \left[g_V^p\,(\nu_\ell)\,ZF_Z(|\vec{q}|^2) + g_V^n NF_N(|\vec{q}|^2)\right], \tag{3.2}$$

is the weak charge of the nucleus. Here, Z and N are the numbers of protons and neutrons in the nucleus, respectively, and g_V^p and g_V^n are the neutrino-proton and neutrino-neutron couplings, respectively. Taking into account radiative corrections in the $\overline{\rm MS}$ scheme [89], accurate values of the vector couplings can be derived as [24][1]

$$g_V^p(\nu_e) = 0.0401, \qquad g_V^p(\nu_\mu) = 0.0318, \qquad g_V^n = -0.5094\,. \tag{3.3}$$

In eq. (3.2), $F_Z(|\vec{q}|^2)$ and $F_N(|\vec{q}|^2)$ are, respectively, the form factors of the proton and neutron distributions in the nucleus, which are the Fourier transforms of the corresponding nucleon distribution in the nucleus and describe the loss of coherence for large values of the momentum transfer $|\vec{q}|$. We use an analytic expression, namely the Helm parameterization [92], for the form factors, that gives practically equivalent results to the other two well known parameterizations, i.e., the symmetrized Fermi [93] and Klein-Nystrand [94] ones. The proton rms radii can be obtained from the muonic atom spectroscopy experiments [95, 96] as explained in ref. [24]

$$R_p({\rm Cs}) = 4.821\ {\rm fm}, \qquad R_p({\rm I}) = 4.766\ {\rm fm}, \qquad R_p({\rm Ar}) = 3.448\ {\rm fm}. \tag{3.4}$$

[1] A different treatment of the hadronic uncertainties is discussed in refs. [90, 91]. The resulting small differences for the values of g_V^p and g_V^n can be neglected in the current analyses of CEνNS data which have other large uncertainties.

JHEP05(2022)109

On the other hand, there is a poor knowledge of the values of the ^{133}Cs, ^{127}I and ^{40}Ar neutron rms radii obtained from the analyses of the COHERENT data [3, 4, 11, 13–15, 24, 97]. The values of these neutron rms radii can, however, be estimated with theoretical calculations based on different nuclear models [24, 27, 98]. Here, we consider the following values obtained from the recent nuclear shell model estimate of the corresponding neutron skins (i.e. the differences between the neutron and the proton rms radii) in ref. [98]

$$R_n(\mathrm{Cs}) \simeq 5.09 \text{ fm}, \qquad R_n(\mathrm{I}) \simeq 5.03 \text{ fm}, \qquad R_n(\mathrm{Ar}) \simeq 3.55 \text{ fm}. \tag{3.5}$$

Following the COHERENT Collaboration [21–23], we take into account the effect of the uncertainty of the values of the neutron rms radii by considering 3.4% and 2% uncertainties for the CsI and Ar CEνNS rates, respectively.

The SM CEνNS differential event rates that are predicted for the COHERENT Ar and CsI detectors are shown in figure 1 as functions of T_{nr}. One can see that there are kinks at $T_{\mathrm{nr}} \approx 50$ keV for Ar and $T_{\mathrm{nr}} \approx 15$ keV for CsI. The steeper slope of the SM differential event rates below these values of T_{nr} is due to the coherency condition $T_{\mathrm{nr}} \lesssim 1/2MR^2$.

The CEνNS cross section is modified if there is a new massive mediator which couples to the SM leptons and quarks. In this work, we focus on two mediator types that have been considered in several previous works [6, 12, 14–16, 19, 25, 26, 70, 71, 99–108]: an additional vector mediator Z' with mass $M_{Z'}$ associated to a new U(1)$'$ gauge group and an additional scalar mediator ϕ with mass M_ϕ. The phenomenology of CEνNS in the specific models that we consider is briefly described in the following two subsections.

3.1 Light vector mediator

The interaction of a Z' vector boson with neutrinos and quarks is described by the generic Lagrangian

$$\mathcal{L}^V_{Z'} = -Z'_\mu \left[\sum_{\ell=e,\mu,\tau} g^{\nu_\ell V}_{Z'} \, \overline{\nu_{\ell L}} \gamma^\mu \nu_{\ell L} + \sum_{q=u,d} g^{qV}_{Z'} \, \overline{q} \gamma^\mu q \right], \tag{3.6}$$

where $g^{qV}_{Z'}$ and $g^{\nu_\ell V}_{Z'}$ are the couplings constants.

In the case of a vector mediator associated with a new U(1)$'$ gauge group, the coupling constants are proportional to the charges Q'_q and Q'_ℓ of quarks and neutrinos under the new gauge symmetry: $g^{qV}_{Z'} = g_{Z'} Q'_q$ and $g^{\nu_\ell V}_{Z'} = g_{Z'} Q'_\ell$, where $g_{Z'}$ is the coupling constant of the symmetry group. Since both the SM and the Z' interactions are of vector type, they contribute coherently to the CEνNS cross section. Moreover, since the vector current is conserved, the proton and neutron coupling are given by the sums of the couplings of their valence quarks. Therefore, the total cross section is obtained by replacing the SM weak charge $Q^V_{\ell,\mathrm{SM}}$ with the new total weak charge (see appendix A)

$$Q^V_{\ell,\mathrm{SM+V}} = Q^V_{\ell,\mathrm{SM}} + \frac{g^2_{Z'} Q'_\ell}{\sqrt{2} G_F \left(|\vec{q}|^2 + M^2_{Z'}\right)} \left[(2Q'_u + Q'_d) \, Z F_Z(|\vec{q}|^2) + (Q'_u + 2Q'_d) \, N F_N(|\vec{q}|^2) \right], \tag{3.7}$$

with $|\vec{q}|^2 \simeq 2MT_{\mathrm{nr}}$.

JHEP05(2022)109

Model	Q'_u	Q'_d	Q'_e	Q'_μ	Q'_τ
universal	1	1	1	1	1
$B-L$	1/3	1/3	−1	−1	−1
$B-3L_e$	1/3	1/3	−3	0	0
$B-3L_\mu$	1/3	1/3	0	−3	0
$B-2L_e-L_\mu$	1/3	1/3	−2	−1	0
$B-L_e-2L_\mu$	1/3	1/3	−1	−2	0
$B_y+L_\mu+L_\tau$	1/3	1/3	0	1	1
L_e-L_μ	0	0	1	−1	0
L_e-L_τ	0	0	1	0	−1
$L_\mu-L_\tau$	0	0	0	1	−1

Table 1. The U(1)′ charges of quarks and leptons in the vector mediator models considered in this work.

In this work we consider the models listed in table 1. There are many models beyond the SM with an additional massive Z' vector boson associated with a new U(1)′ gauge symmetry (see, e.g., the review in ref. [69]). A necessary requirement is that the theory is anomaly-free. However, it is possible to consider effective anomalous models that describe the interactions of SM fermions with the implicit requirement that the anomalies are canceled by the contributions of the non-standard fermions of the full theory. This is the case of the first model that we consider: a Z' boson which couples universally to all SM fermions [6, 12, 14, 15, 26, 70, 71]. In this case $Q'_\ell = Q'_u = Q'_d = 1$, and the coupling is same for all the fermions.

Other models that we consider are anomaly-free if the SM is extended with the introduction of three right-handed neutrinos (see, e.g., ref. [109]), which are also beneficial for the generation of the neutrino masses that are necessary for the explanation of the oscillations of neutrinos observed in many experiments (see, e.g., refs. [85, 110]). In this case, there is an infinite set of anomaly-free U(1)′ gauge groups generated by

$$G(c_1, c_2, c_3, c_e, c_\mu, c_\tau) = c_1 B_1 + c_2 B_2 + c_3 B_3 - c_e L_e - c_\mu L_\mu - c_\tau L_\tau, \tag{3.8}$$

where B_1, B_2, and B_3 are the baryon numbers of the three generations and L_α are the lepton numbers for $\alpha = e, \mu, \tau$. We assume that for each generation the U(1)′ couplings of the right-handed neutrino is the same as that of the left-handed neutrino in order to have vectorial U(1)′ interactions. Therefore, when we extend the SM gauge group $\mathrm{SU}(3)_C \times \mathrm{SU}(2)_L \times \mathrm{U}(1)_Y$ to $\mathrm{SU}(3)_C \times \mathrm{SU}(2)_L \times \mathrm{U}(1)_Y \times \mathrm{U}(1)'$, there are no $[\mathrm{SU}(3)_C]^2\mathrm{U}(1)_Y$, $[\mathrm{U}(1)']^3$ and $[\text{gravity}]^2\mathrm{U}(1)'$ anomalies, because of the vectorial character of the involved interactions. The $[\mathrm{U}(1)']^2\mathrm{U}(1)_Y$ anomaly cancels because for each generation the difference

JHEP05(2022)109

of the Y charges of left-handed and right-handed quarks (leptons) is zero. The remaining $[\mathrm{SU}(2)_L]^2\mathrm{U}(1)'$ and $[\mathrm{U}(1)_Y]^2\mathrm{U}(1)'$ anomalies are canceled with the constraint

$$c_1 + c_2 + c_3 - c_e - c_\mu - c_\tau = 0. \tag{3.9}$$

It is often assumed that the quark charges are universal, in order to avoid unobserved flavor-changing neutral currents in the quark sector. In this case, we have

$$G_B(c_B, c_e, c_\mu, c_\tau) = c_B B - c_e L_e - c_\mu L_\mu - c_\tau L_\tau, \tag{3.10}$$

with the constraint (see, e.g., refs. [111, 112])

$$3c_B - c_e - c_\mu - c_\tau = 0. \tag{3.11}$$

Here $B = B_1 + B_2 + B_3$ is the usual baryon number.

We consider the following anomaly-free models that correspond to different choices of the coefficients in eq. (3.8) or (3.10) and contribute to CEνNS interactions of ν_e and ν_μ:

$B - L = G_B(1, 1, 1, 1)$. Here $L = L_e + L_\mu + L_\tau$ is the total lepton number. This is the most popular Z' model, with a huge literature (see, e.g., the reviews in refs. [69, 72, 73]). It was considered recently in several CEνNS phenomenological analyses, e.g. those in refs. [25, 26, 71, 104, 113]. Note that, since there are no ν_τ's in the COHERENT neutrino beam, bounds on the coupling constant in the anomaly-free model generated by

$$G_B(1, 3/2, 3/2, 0) = B - \frac{3}{2}\left(L_e + L_\mu\right), \tag{3.12}$$

considered, e.g., in ref. [102], can be obtained from the bounds on the coupling constant $g_{Z'}$ in the $B - L$ model by rescaling it by the factor $\sqrt{2/3}$, because the ν_e and ν_μ couplings are changed by the same factor 3/2.

$B_y + L_\mu + L_\tau = G(1, -y, y - 3, 0, -1, -1)$. In this model, proposed in ref. [114] and considered, e.g., in ref. [113], $B_y = B_1 - yB_2 + (y - 3)B_3$.

$B - 3L_e = G_B(1, 3, 0, 0)$. This model was considered, e.g., in refs. [102, 104, 113, 115]. In this case, only the ν_e CEνNS cross section is affected by the new Z'-mediated interaction. Moreover, since there are no ν_τ's in the COHERENT neutrino beam, the bounds on the coupling constant $g_{Z'}$ obtained in this model can be extended to all the anomaly-free models generated by

$$G_B(1, 3w_e, 0, 3(1 - w_e)) = B - 3w_e L_e - 3(1 - w_e)L_\tau \tag{3.13}$$

through a rescaling of the coupling constant by a factor $1/\sqrt{w_e}$.

$B - 3L_\mu = G_B(1, 0, 3, 0)$. This model was considered, e.g., in refs. [104, 113, 115]. In this case, only the ν_μ CEνNS cross section is affected by the new Z'-mediated interaction and, in analogy with the argument in the previous item, the bounds on the coupling

JHEP05(2022)109

constant $g_{Z'}$ obtained in this model can be extended to all the anomaly-free models generated by

$$G_B(1, 0, 3w_\mu, 3(1 - w_\mu)) = B - 3w_\mu L_\mu - 3(1 - w_\mu)L_\tau \tag{3.14}$$

through a rescaling of the coupling constant by a factor $1/\sqrt{w_\mu}$. For example, the $B - (3/2)(L_\mu + L_\tau)$ considered in refs. [113, 115] is obtained with $w_\mu = 1/2$.

$B - 2L_e - L_\mu = G_B(1, 2, 1, 0)$. This model was considered, e.g., in ref. [104]. In analogy with the discussion in the previous items, the bounds on the coupling constant $g_{Z'}$ obtained in this model can be extended to all the anomaly-free models generated by

$$G_B(1, 2w_1, w_1, 3(1 - w_1)) = B - 2w_1 L_e - w_1 L_\mu - 3(1 - w_1)L_\tau \tag{3.15}$$

through a rescaling of the coupling constant by a factor $1/\sqrt{w_1}$.

$B - L_e - 2L_\mu = G_B(1, 1, 2, 0)$. This model, was considered, e.g., in ref. [104]. Again, in analogy with the discussion in the previous items, the bounds on the coupling constant $g_{Z'}$ obtained in this model can be extended to all the anomaly-free models generated by

$$G_B(1, w_2, 2w_2, 3(1 - w_2)) = B - w_2 L_e - 2w_2 L_\mu - 3(1 - w_2)L_\tau \tag{3.16}$$

through a rescaling of the coupling constant by a factor $1/\sqrt{w_2}$.

The effects of the models above on the CEνNS differential event rates that are predicted for the COHERENT Ar and CsI detectors are illustrated, respectively, in figures 1a and 1b. In these figures we choose $g_{Z'} = 10^{-4}$ and $M_{Z'} = 10$ MeV and we compared the model predictions with the SM one. One can see that the effects of the light mediator are similar for the Ar and CsI detectors and the vector boson mediator contribution increases for small values of $T_{\rm nr} \simeq |\vec{q}|^2/2M$ because of the propagator in eq. (3.7). The different scales of $T_{\rm nr}$ in figures 1a and 1b are obviously due to the different masses of the nuclei.

In the case of the universal Z' model there is a deep dip due to a cancellation between the negative SM and the positive Z' contributions to the weak charge in eq. (3.7). This occurs only in the universal model because only in this case all the quark and lepton charges are positive and both ν_e and ν_μ interact with the Z'. Indeed, there is a cancellation for

$$T_{\rm nr} = -\frac{1}{2M}\left(\frac{3g_{Z'}^2}{\sqrt{2}G_F}\frac{ZF_Z(|\vec{q}|^2) + NF_N(|\vec{q}|^2)}{g_V^p ZF_Z(|\vec{q}|^2) + g_V^n NF_N(|\vec{q}|^2)} + M_{Z'}^2\right), \tag{3.17}$$

which occurs at $T_{\rm nr} \simeq 92$ keV for Ar in figure 1a and $T_{\rm nr} \simeq 27$ keV for CsI in figure 1b.

There is a cancellation for ν_μ also in the $B_y + L_\mu + L_\tau$ model, since the quarks and ν_μ have positive charges (see table 1). The cancellation occurs at

$$T_{\rm nr} = -\frac{1}{2M}\left(\frac{g_{Z'}^2}{\sqrt{2}G_F}\frac{ZF_Z(|\vec{q}|^2) + NF_N(|\vec{q}|^2)}{g_V^p ZF_Z(|\vec{q}|^2) + g_V^n NF_N(|\vec{q}|^2)} + M_{Z'}^2\right), \tag{3.18}$$

JHEP05(2022)109

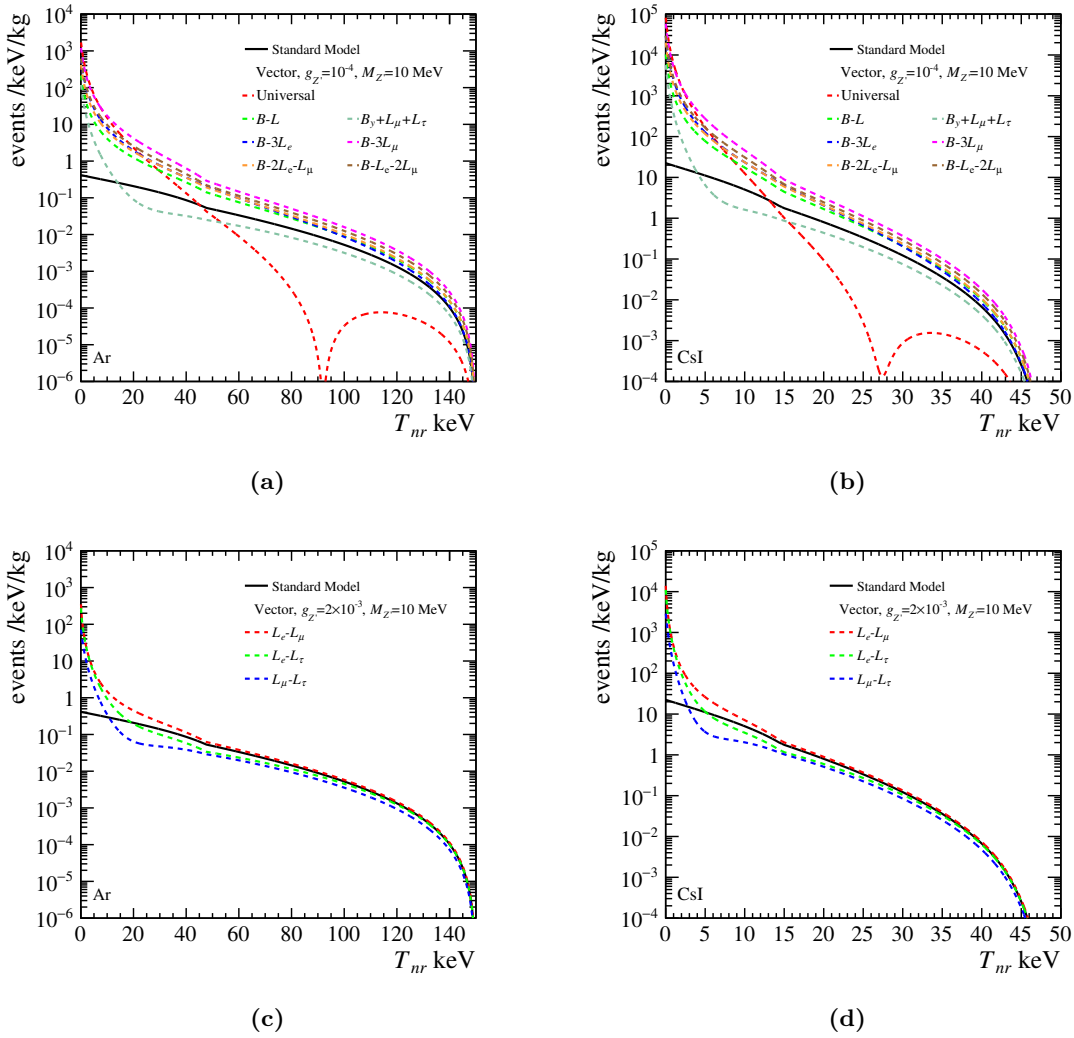

Figure 1. Predicted CEνNS differential event rates corresponding to the experimental configuration and data taking time of the COHERENT Ar (a, c) and CsI (b, d) detectors in the vector mediator models considered in this work.

which corresponds to $T_{\rm nr} \simeq 29$ keV for Ar in figure 1a and $T_{\rm nr} \simeq 8$ keV for CsI in figure 1b. Since in this case there is no cancellation of the SM contribution of ν_e, which does not interact with the Z', there are only shallow dips at these energies in figures 1a and 1b for this model. Note that the total differential rate is smaller than the SM differential rate for energies above the dip, because the positive and smaller Z' contribution to $Q^V_{\mu,\rm SM+V}$ is added to the dominant negative SM contribution, decreasing the absolute value of $Q^V_{\mu,\rm SM+V}$.

In all the other models above the quarks and leptons have opposite charges (see table 1) and the Z' contribution to the weak charge in eq. (3.7) is negative as the SM contribution. Therefore, the total differential rate is larger than the SM rate for all values of $T_{\rm nr}$, as shown in figures 1a and 1b.

JHEP05(2022)109

We also consider the following three possible $L_\alpha - L_\beta$ models that are anomaly-free and can be gauged without extending the SM content with right-handed neutrinos [74–77]:

$L_e - L_\mu = G_B(0,-1,1,0)$. This model, obtained from eq. (3.10) with $c_B = 0$, $c_e = -1$ $c_\mu = 1$, and $c_\tau = 0$, was considered, e.g., in refs. [76, 113, 116].

$L_e - L_\tau = G_B(0,-1,0,1)$. This model, obtained from eq. (3.10) with $c_B = 0$, $c_e = -1$ $c_\mu = 0$, and $c_\tau = 1$, was considered, e.g., in refs. [76, 113, 116].

$L_\mu - L_\tau = G_B(0,0,-1,1)$. This model, obtained from eq. (3.10) with $c_B = 0$, $c_e = 0$ $c_\mu = -1$, and $c_\tau = 1$, was considered in many papers, e.g., in refs. [26, 28, 59, 71, 76, 78, 79, 117].

Since in these models the Z' vector boson does not couple to quarks, there are no tree-level interactions that contribute to CEνNS (assuming the absence of tree-level kinetic mixing). However, there is kinetic mixing of the Z' and the photon at the one-loop level that induces a contribution to CEνNS through the photon interaction with quarks [28, 78, 79]. The CEνNS cross section in these three models is [26, 78][2]

$$\left(\frac{d\sigma}{dT_{\rm nr}}\right)^{\nu_\ell-\mathcal{N}}_{L_\alpha-L_\beta}(E,T_{\rm nr}) = \frac{G_F^2 M}{\pi}\left(1-\frac{MT_{\rm nr}}{2E^2}\right) \times\left\{\left[g_V^p\,(\nu_\ell)+\frac{\sqrt{2}\alpha_{\rm EM}g_{Z'}^2\left(\delta_{\ell\alpha}\varepsilon_{\beta\alpha}(|\vec{q}|)+\delta_{\ell\beta}\varepsilon_{\alpha\beta}(|\vec{q}|)\right)}{\pi G_F\left(|\vec{q}|^2+M_{Z'}^2\right)}\right]ZF_Z(|\vec{q}|^2)+g_V^n NF_N(|\vec{q}|^2)\right\}^2, \tag{3.19}$$

where $\alpha_{\rm EM}$ is the electromagnetic fine-structure constant and $\varepsilon_{\beta\alpha}(|\vec{q}|)$ is the one-loop kinetic mixing coupling, that is given by [28, 79]

$$\varepsilon_{\beta\alpha}(|\vec{q}|) = \int_0^1 x(1-x)\ln\left(\frac{m_\beta^2+x(1-x)|\vec{q}|^2}{m_\alpha^2+x(1-x)|\vec{q}|^2}\right)dx\,, \tag{3.20}$$

where m_β and m_α are the charged lepton masses and we took into account that for CEνNS $q^2 \simeq -|\vec{q}|^2 \simeq -2MT_{\rm nr}$. Note that the Z' contribution is invariant for $\alpha \leftrightarrows \beta$, as it should be, since $L_\alpha - L_\beta$ and $L_\beta - L_\alpha$ are physically equivalent. Note also that the sign of the loop contribution of the i charged lepton to ν_ℓ scattering is given by $-Q'_iQ'_\ell$, where the minus comes from the negative electric charge of the charged lepton propagating in the loop. Therefore, the mass of the charged lepton with the same flavor ℓ of the scattering neutrino is always at the denominator of the logarithm in eq. (3.20) and the mass of the other charged lepton taking part to the new symmetry is always at the numerator. Figure 2 shows the value of $\varepsilon_{\beta\alpha}(|\vec{q}|)$ for each of the three $L_\alpha - L_\beta$ symmetries as a function of $|\vec{q}|$ in the range of the COHERENT CEνNS. One can see that only $\varepsilon_{\tau\mu}$ is almost constant, because $|\vec{q}| \ll m_\tau$ and $|\vec{q}| < m_\mu$. In this case it is possible to approximate $\varepsilon_{\tau\mu} \simeq \ln(m_\tau^2/m_\mu^2)/6$, as done in refs. [26, 71, 78]. On the other hand, for the symmetries $L_e - L_\mu$ and $L_e - L_\tau$ the $|\vec{q}|$ dependence of $\varepsilon_{\beta\alpha}$ on $|\vec{q}|$ must be taken into account, because $|\vec{q}| \gg m_e$.

[2]We correct here the sign of the Z' contribution with respect to that used in ref. [26]. Let us also note that in the analysis in ref. [28] the Z' contribution has the correct sign, but there is an additional factor 1/2 that is incorrect, as shown in appendix A.

JHEP05(2022)109

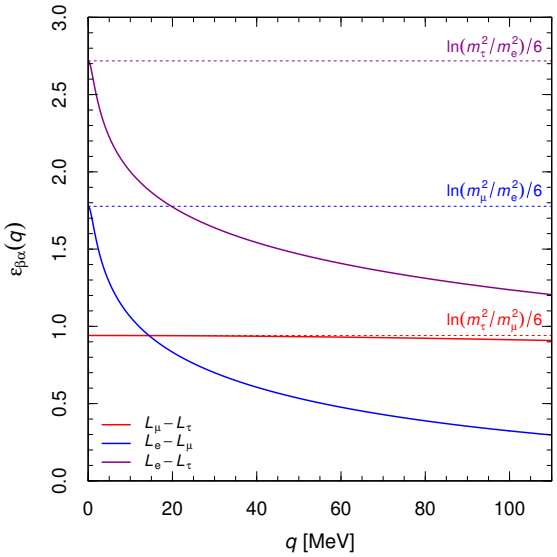

Figure 2. Values of $\varepsilon_{\beta\alpha}$ in eq. (3.20) for each of the three $L_\alpha - L_\beta$ symmetries as a function of $q = |\vec{q}| \simeq \sqrt{2MT_{\rm nr}}$ in the range of the COHERENT CEνNS data.

Figures 1c and 1d illustrate the effects of the Z' contribution to the CEνNS differential event rates that are predicted for the COHERENT Ar and CsI detectors in the $L_\alpha - L_\beta$ models. In these figures we choose $g_{Z'} = 2 \times 10^{-3}$ and $M_{Z'} = 10$ MeV and we compared the model predictions with that of the SM. One can see that, as for the models in figures 1a and 1b discussed above, the effects of the light mediator are similar for the Ar and CsI detectors and the vector boson mediator contribution increases for small values of $T_{\rm nr} \simeq |\vec{q}|^2/2M$ because of the propagator in eq. (3.7).

In the case of the $L_\mu - L_\tau$ model the Z' contribution to $Q^V_{\mu,\rm SM+V}$ is positive and there can be a cancellation with the negative SM contribution. The cancellation occurs at

$$T_{\rm nr} = -\frac{1}{2M}\left(\frac{\alpha_{\rm EM} g^2_{Z'}}{3\pi\sqrt{2}G_F}\,\ln\!\left(\frac{m_\tau^2}{m_\mu^2}\right)\frac{ZF_Z(|\vec{q}|^2)}{g_V^p ZF_Z(|\vec{q}|^2) + g_V^n NF_N(|\vec{q}|^2)} + M^2_{Z'}\right), \tag{3.21}$$

which corresponds to $T_{\rm nr} \simeq 23$ keV for Ar in figure 1c and $T_{\rm nr} \simeq 6$ keV for CsI in figure 1d. Since there is no cancellation of the SM contribution of ν_e, which does not interact with the Z', there are only shallow dips at these energies in figures 1c and 1d for this model. The total differential rate is smaller than the SM differential rate for energies above the dip for the same reason that has been discussed above for the $B_y + L_\mu + L_\tau$ model.

In the case of the $L_e - L_\tau$ model, there can be a cancellation of the positive Z' contribution to $Q^V_{e,\rm SM+V}$ with the negative SM contribution, but it is difficult to estimate for which value of $T_{\rm nr}$ because of the strong dependence of $\varepsilon_{\tau e}$ on $T_{\rm nr} \simeq |\vec{q}|^2/2M$ shown in figure 2. However, one can see from figures 1c and 1d that there are shallow dips of the differential rates at values of $T_{\rm nr}$ that are larger than in the $L_\mu - L_\tau$ model, because $\varepsilon_{\tau e} > \varepsilon_{\tau\mu}$, as shown in figure 2. The dip is more shallow than in the $L_\mu - L_\tau$ model because the ν_e contribution to the CEνNS event rate is smaller than the sum of the ν_μ and $\bar{\nu}_\mu$ contributions.

JHEP05(2022)109

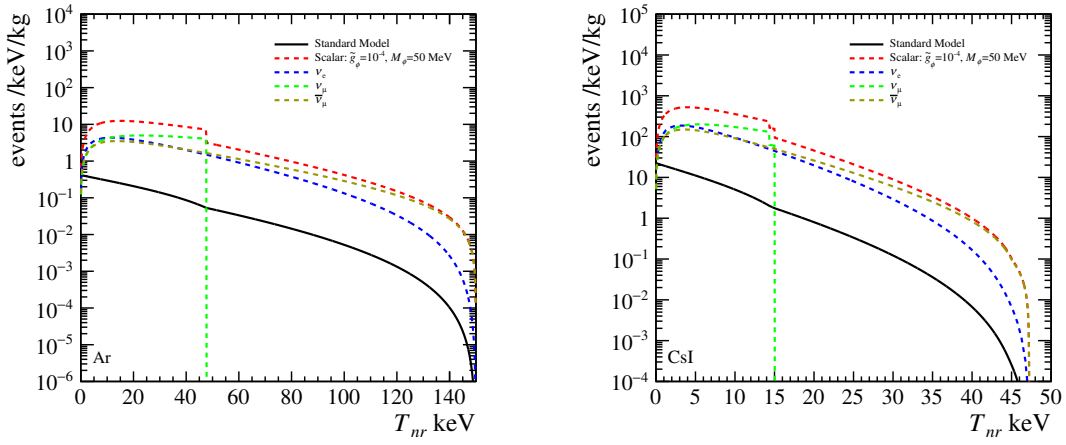

(a) **(b)**

Figure 3. Predicted CEνNS differential event rates corresponding to the experimental configuration and data taking time of the COHERENT Ar (a) and CsI (b) detectors in the universal scalar mediator model.

In the case of the $L_e - L_\mu$ model, the situation is more complicated, because the Z' contribution to $Q^V_{e,\mathrm{SM+V}}$ is positive, since $\varepsilon_{\mu e} > 0$, but the Z' contribution to $Q^V_{\mu,\mathrm{SM+V}}$ is negative, since $\varepsilon_{e\mu} < 0$. Therefore, the Z' contributions of the dominant ν_μ and $\bar{\nu}_\mu$ fluxes enhance the CEνNS differential event rate with respect to the SM prediction, whereas the subdominant ν_e flux generate a decrease for sufficiently large values of T_{nr} (about 40 keV for Ar in figure 1c and 15 keV for CsI in figure 1d) As a result of these opposite contributions, the total CEνNS differential rates of the $L_e - L_\mu$ model shown in figures 1c and 1d are only slightly larger than the SM rates in the large-T_{nr} parts of the figures.

3.2 Light scalar mediator

Non-standard neutrino interactions mediated by a scalar boson ϕ are possible if the SM fermion content is extended with the addition of right-handed neutrinos. The generic Lagrangian that describes the interaction of ϕ with neutrinos and quarks is

$$\mathcal{L}^S_\phi = -\phi \left[\sum_{\ell=e,\mu,\tau} g^{\nu_\ell}_\phi \, \overline{\nu_\ell} \, \nu_\ell + \sum_{q=u,d} g^q_\phi \, \overline{q} \, q \right], \tag{3.22}$$

where $\nu_\ell = \nu_{\ell L} + \nu_{\ell R}$ and $g^{\nu_\ell}_\phi$ and g^q_ϕ are the coupling constants. The contribution of the scalar boson interaction to the CEνNS cross section adds incoherently to the SM cross section [7, 10, 80–82]

$$\frac{d\sigma_{\nu_\ell\text{-}\mathcal{N}}}{dT_{\mathrm{nr}}} = \left(\frac{d\sigma_{\nu_\ell\text{-}\mathcal{N}}}{dT_{\mathrm{nr}}}\right)_{\mathrm{SM}} + \left(\frac{d\sigma_{\nu_\ell\text{-}\mathcal{N}}}{dT_{\mathrm{nr}}}\right)_{\mathrm{scalar}}, \tag{3.23}$$

with

$$\left(\frac{d\sigma_{\nu_\ell\text{-}\mathcal{N}}}{dT_{\mathrm{nr}}}\right)_{\mathrm{scalar}} = \frac{M^2 T_{\mathrm{nr}}}{4\pi E^2} \frac{(g^{\nu_\ell}_\phi)^2 \mathcal{Q}^2_\phi}{(|\vec{q}|^2 + M^2_\phi)^2}, \tag{3.24}$$

JHEP05(2022)109

where $\mathcal{Q}_\phi$ is the scalar charge of the nucleus, given by

$$\mathcal{Q}_\phi = ZF_Z(|\vec{q}|^2) \sum_{q=u,d} g_\phi^q \langle p|\bar{q}q|p\rangle + NF_N(|\vec{q}|^2) \sum_{q=u,d} g_\phi^q \langle n|\bar{q}q|n\rangle. \tag{3.25}$$

It is sometimes written as [10, 80–82]

$$\mathcal{Q}_\phi = ZF_Z(|\vec{q}|^2) \sum_{q=u,d} g_\phi^q \frac{m_p}{m_q} f_q^p + NF_N(|\vec{q}|^2) \sum_{q=u,d} g_\phi^q \frac{m_n}{m_q} f_q^n, \tag{3.26}$$

with the quark contributions to the nucleon masses

$$f_q^{\mathbb{N}} = \frac{m_q}{m_n} \langle \mathbb{N}|\bar{q}q|\mathbb{N}\rangle, \tag{3.27}$$

for $\mathbb{N} = p, n$. Since the scalar currents are not conserved, the scalar charges of the nucleons are not simply given by the sums of the charges of their valence quarks, as in the case of a vector boson mediator (see eq. (3.7)). The proton and neutron matrix elements of the scalar quark current must be calculated (see, e.g., the recent refs. [118–121]). For simplicity, we consider equal couplings for the u and d quarks and equal couplings for ν_e and ν_μ

$$g_\phi^u = g_\phi^d = g_\phi^q \quad \text{and} \quad g_\phi^{\nu_e} = g_\phi^{\nu_\mu} = g_\phi^\nu. \tag{3.28}$$

Then, we have

$$\mathcal{Q}_\phi = g_\phi^q \left[ZF_Z(|\vec{q}|^2) \langle p|\bar{u}u + \bar{d}d|p\rangle + NF_N(|\vec{q}|^2) \langle n|\bar{u}u + \bar{d}d|n\rangle \right]. \tag{3.29}$$

Considering the isospin approximation, we obtain[3]

$$\langle p|\bar{u}u + \bar{d}d|p\rangle = \langle n|\bar{u}u + \bar{d}d|n\rangle = \langle N|\bar{u}u + \bar{d}d|N\rangle = \frac{\sigma_{\pi N}}{\overline{m}_{ud}}, \tag{3.30}$$

where $\overline{m}_{ud} = (m_u + m_d)/2$ and $\sigma_{\pi N}$ is the pion-nucleon σ-term that has been determined in different ways in the literature (see the recent review in ref. [122]). Recent values have been obtained from pionic atoms and pion-nucleon scattering [118, 123, 124] and from lattice calculations [119, 121]. Since there are large uncertainties on the values of $\sigma_{\pi N}$ and $\overline{m}_{ud}$, we choose a reference value for $\sigma_{\pi N}/\overline{m}_{ud}$ given by the ratio of the central value of $\sigma_{\pi N}$ determined in ref. [118] ($\sigma_{\pi N} = 59.1\,\text{MeV}$) and the central PDG values [85] $m_u = 2.16\,\text{MeV}$ $m_d = 4.67\,\text{MeV}$, that gives

$$\left(\frac{\sigma_{\pi N}}{\overline{m}_{ud}}\right)_{\text{ref}} = 17.3, \tag{3.31}$$

that allows us to write the scalar cross section (3.24) as

$$\left(\frac{d\sigma_{\nu_\ell\text{-}\mathcal{N}}}{dT_{\text{nr}}}\right)_{\text{scalar}} = \frac{M^2 T_{\text{nr}}}{4\pi E^2} \frac{\tilde{g}_\phi^4}{(|\vec{q}|^2 + M_\phi^2)^2} \left(\frac{\sigma_{\pi N}}{\overline{m}_{ud}}\right)_{\text{ref}}^2 \left[ZF_Z(|\vec{q}|^2) + NF_N(|\vec{q}|^2)\right]^2, \tag{3.32}$$

with

$$\tilde{g}_\phi^2 = g_\phi^{\nu_\ell} g_\phi^q \frac{\sigma_{\pi N}/\overline{m}_{ud}}{(\sigma_{\pi N}/\overline{m}_{ud})_{\text{ref}}}. \tag{3.33}$$

[3] We neglect the small $|\vec{q}|$-dependent corrections discussed in ref. [98].

JHEP05(2022)109

In this way the results of other calculations can be compared with our results by appropriate rescaling of $\tilde{g}_\phi$ according with the assumptions. We guess that $\tilde{g}_\phi$ is practically equal to g_ϕ in ref. [25], where the expression (3.26) was used for the scalar charge of the nucleus, with the values of the $f_q^{\mathbb{N}}$'s given in ref. [118], although the assumed values of the quark masses are not specified. Indeed, the values of the $f_q^{\mathbb{N}}$'s in ref. [118] have been obtained from the value of $\sigma_{\pi N}$ using eq. (13) of ref. [125], which implies

$$\sum_{q=u,d} \frac{m_p}{m_q} f_q^p = \sum_{q=u,d} \frac{m_n}{m_q} f_q^n = \frac{\sigma_{\pi N}}{\overline{m}_{ud}}. \tag{3.34}$$

On the other hand, our approach is different from that in refs. [15, 80, 126], which considered different values for the proton and neutron matrix elements in eq. (3.29): $\langle p|\bar{u}u+\bar{d}d|p\rangle = 15.1$ and $\langle n|\bar{u}u+\bar{d}d|n\rangle = 14$. These values correspond to a rather large 8% violation of the isospin symmetry.

Let us also note that our treatment neglected the contribution of the strange and heavier quarks, whose contributions to the nucleon mass have very large uncertainties (see, e.g., table 4 of ref. [127]). If one wants to consider them, their contributions can be taken into account by rescaling appropriately $\tilde{g}_\phi$, assuming that the coupling of ϕ with all quarks is the same.

Figure 3 illustrates the effect of the scalar boson mediator on the CEνNS differential event rates that are predicted for the COHERENT Ar and CsI detectors for $\tilde{g}_\phi = 10^{-4}$ and $M_\phi = 50$ MeV. One can see that the total CEνNS rates are larger than the SM rates for all values of $T_{\rm nr}$, because the scalar boson cross section adds incoherently to the SM cross section, according to eq. (3.23). In the two panels of figure 3 one can also notice that the total CEνNS rates represented by the red-dashed lines have small discontinuities at $T_{\rm nr} = 47.7$ keV for Ar and $T_{\rm nr} \simeq 15$ keV for CsI. These values correspond to the maximum nuclear kinetic energy $T_{\rm nr}^{\rm max} = 2E^2/M$ for the monoenergetic ν_μ from pion decay ($E = 29.8$ MeV), as shown by the green-dashed lines that represent the ν_μ contributions. One can see that there is an effect also for the SM differential event rates, which change slope at the same values of $T_{\rm nr}$. The effect for the scalar boson contribution is larger because it is enhanced by the $T_{\rm nr}$ in the numerator of the scalar cross section, see eq. (3.24). Such a dependence causes also the decrease of the scalar contribution for very low values of $T_{\rm nr}$ that is visible in figure 3.

4 Constraints on light mediator models

In this section we present the results of the analyses of the COHERENT CsI and Ar data with the light-mediator models described in section 3. Since the data are fitted well by the SM CEνNS prediction, we obtain constraints on the mass and coupling of the light mediator in each model. Let us note that the constraints that can be obtained with previous COHERENT CsI and Ar data have been presented in refs. [6, 9, 16, 19, 26, 28] for the more popular universal, $B-L$, and $L_\mu - L_\tau$ models and in ref. [113] for the $B-3L_e$, $B-3L_\mu$, and $B_y + L_\mu + L_\tau$ models.

In the following subsections, we present the 2σ (95.45% C.L.) limits obtained from the COHERENT Ar and CsI data for the models discussed in section 3 and we compare

JHEP05(2022)109

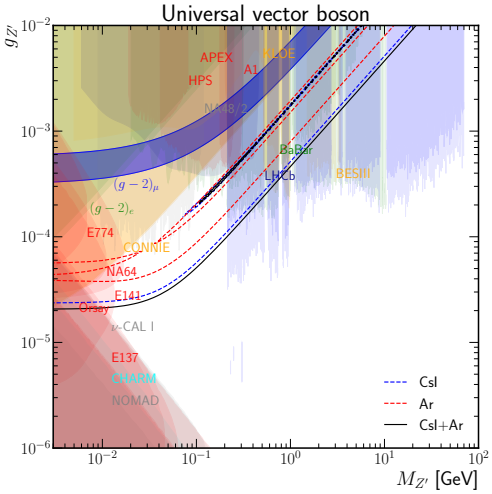

Figure 4. Excluded regions (2σ) in the $M_{Z'}$-$g_{Z'}$ plane for the universal vector mediator model.

them with the constraints of other experiments by using the **darkcast** [128] code for recasting the limits in the different models under consideration. In particular, we compare the constraints on the light vector boson mediator obtained from the COHERENT data with the excluded regions obtained from searches of visible dark photon decays in beam dump (E141 [129], E137 [130], E774 [131], KEK [132], Orsay [133–135], ν-CAL I [136–139], CHARM [140, 141], NOMAD [142], and PS191 [143, 144]), fixed target (A1 [145] and APEX [146]), collider (BaBar [147], KLOE [148, 149], LHCb [150]), and rare-meson-decay (NA48/2 [151]) experiments, and searches of invisible dark photons decays in the NA64 [152] and BaBar [153] experiments. We also compare the constraints with the excluded regions obtained from the global analysis of oscillation data (OSC) [113].

4.1 Universal Z' model

Figure 4 shows the 2σ limits that we obtained from the COHERENT Ar and CsI data for the universal Z' model [6, 12, 14, 15, 26, 70, 71]. The black line delimits the 2σ allowed regions obtained from the combined analysis of the CsI and Ar data, while the blue and red lines delimit the excluded regions obtained from the CsI and Ar data, respectively.

Considering the combined analysis of the CsI and Ar data, one can see that in the low-mass region the black line, which represents the upper boundary of the 2σ allowed region, flattens due to the fact that the contribution of the Z' boson to $Q^V_{\ell,\mathrm{SM+V}}$ is small. This happens for $M_{Z'} \ll 100$ MeV, because $g_{Z'}$ is small and the boundary does not depend on $M_{Z'}$ since $|\vec{q}| \gg M_{Z'}$ in the Z' boson propagator. On the other hand, for higher masses the contribution of the Z' boson is suppressed by a large $M_{Z'}$, which is dominant in the propagator, and the boundary is given by a diagonal line proportional to $M_{Z'}$. The numerical values of the 2σ limits in these two simple cases are given in table 2.

In the upper-middle part of figure 4, one can see that another black line delimits a thin diagonal strip, where $Q^V_{\ell,\mathrm{SM+V}} \simeq -Q^V_{\mathrm{SM}}$, corresponding to a degeneracy with the SM

JHEP05(2022)109

model	Ar		CsI		CsI+Ar	
	$g_{Z'}$(low $M_{Z'}$)	$\frac{g_{Z'}}{M_{Z'}}$(high $M_{Z'}$)	$g_{Z'}$(low $M_{Z'}$)	$\frac{g_{Z'}}{M_{Z'}}$(high $M_{Z'}$)	$g_{Z'}$(low $M_{Z'}$)	$\frac{g_{Z'}}{M_{Z'}}$(high $M_{Z'}$)
universal	3.91×10^{-5}	0.82×10^{-3}	2.36×10^{-5}	0.53×10^{-3}	2.07×10^{-5}	0.48×10^{-3}
$B-L$	5.35×10^{-5}	1.67×10^{-3}	5.27×10^{-5}	1.00×10^{-3}	4.42×10^{-5}	0.99×10^{-3}
$B_y+L_\mu+L_\tau$	10.4×10^{-5}	3.58×10^{-3}	4.97×10^{-5}	1.14×10^{-3}	4.47×10^{-5}	1.04×10^{-3}
$B-3L_e$	4.91×10^{-5}	1.55×10^{-3}	5.16×10^{-5}	0.96×10^{-3}	4.34×10^{-5}	0.95×10^{-3}
$B-3L_\mu$	3.45×10^{-5}	1.09×10^{-3}	3.21×10^{-5}	0.64×10^{-3}	2.76×10^{-5}	0.63×10^{-3}
$B-2L_e-L_\mu$	4.62×10^{-5}	1.48×10^{-3}	4.79×10^{-5}	0.89×10^{-3}	3.95×10^{-5}	0.88×10^{-3}
$B-L_e-2L_\mu$	3.97×10^{-5}	1.28×10^{-3}	3.86×10^{-5}	0.75×10^{-3}	3.26×10^{-5}	0.74×10^{-3}
L_e-L_μ	161×10^{-5}	54.2×10^{-3}	166×10^{-5}	36.1×10^{-3}	137×10^{-5}	34.9×10^{-3}
L_e-L_τ	204×10^{-5}	71.1×10^{-3}	140×10^{-5}	29.9×10^{-3}	125×10^{-5}	26.6×10^{-3}
$L_\mu-L_\tau$	234×10^{-5}	80.9×10^{-3}	116×10^{-5}	26.6×10^{-3}	103×10^{-5}	24.2×10^{-3}
	$\tilde{g}_\phi$(low M_ϕ)	$\frac{\tilde{g}_\phi}{M_\phi}$(high M_ϕ)	$\tilde{g}_\phi$(low M_ϕ)	$\frac{\tilde{g}_\phi}{M_\phi}$(high M_ϕ)	$\tilde{g}_\phi$(low M_ϕ)	$\frac{\tilde{g}_\phi}{M_\phi}$(high M_ϕ)
scalar	2.30×10^{-5}	0.58×10^{-3}	1.80×10^{-5}	0.31×10^{-3}	1.68×10^{-5}	0.30×10^{-3}

Table 2. The 2σ (95.45% C.L.) upper bounds on the coupling of the new boson mediator obtained from the separate and combined analyses of the Ar and CsI COHERENT CEνNS data for low and high values of the boson mass in the models considered in this paper. $g_{Z'}/M_{Z'}$ and $\tilde{g}_\phi/M_\phi$ are in units of GeV^{-1}.

cross section, as explained in ref. [26]. Neglecting the form factors and the small proton SM contribution, one can find that the thin allowed strip corresponds to

$$(g_{Z'}^{\rm univ})_{\rm strip} \simeq \sqrt{\frac{N}{A}\frac{\sqrt{2}G_F M_{Z'}^2}{3}} \simeq 1.8\times10^{-3}\,\frac{M_{Z'}}{\rm GeV}, \tag{4.1}$$

taking into account that $(N/A)_{\rm Ar} \simeq (N/A)_{\rm CsI} \simeq 0.58$. Note that the existence of the allowed strip in the universal model is related to the possibility to have a cancellation of the CEνNS differential event rate discussed in section 3 (see eq. (3.17)) because it is a consequence of the different signs of the SM and Z' contributions to $Q^V_{\ell,{\rm SM+V}}$. Indeed, all the models that can have a cancellation of the CEνNS differential as discussed in section 3 (i.e. the universal, $B_y+L_\mu+L_\tau$, L_e-L_τ, and $L_\mu-L_\tau$ models) have an allowed strip, as discussed in the following. The cancellation occurs in the excluded parameter space between the lower allowed region and the thin allowed strip for

$$(g_{Z'}^{\rm univ})_{\rm canc} \simeq \sqrt{\frac{N}{A}\frac{\sqrt{2}G_F M_{Z'}^2}{6}} \simeq 1.3\times10^{-3}\,\frac{M_{Z'}}{\rm GeV}, \tag{4.2}$$

where we neglected the form factors and the small proton SM contribution.

One can see from figure 4 that the limits obtained from the CsI data are stricter than those obtained from the Ar data and are close to those of the combined fit. The limits obtained from the analysis of the Ar data are more complicated and one can see that there

JHEP05(2022)109

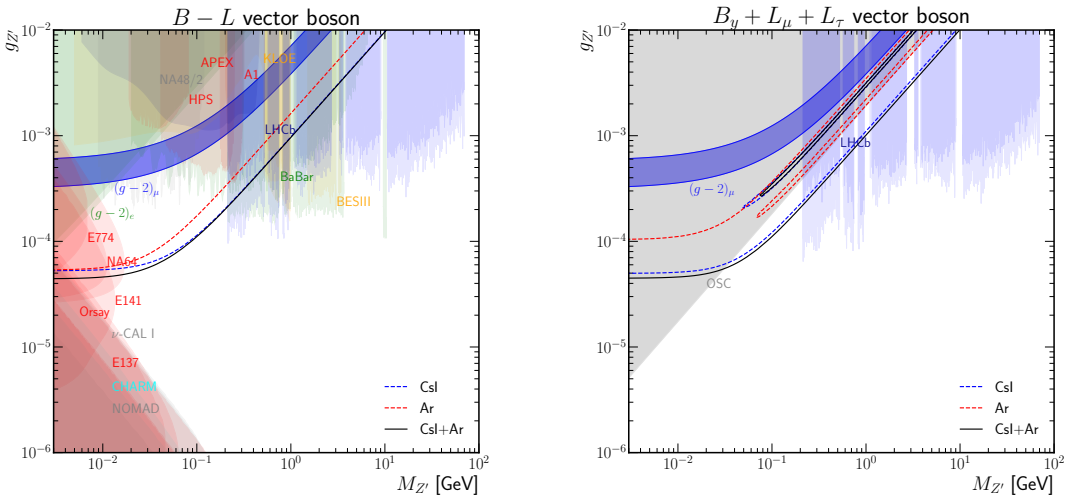

(a) **(b)**

Figure 5. Excluded regions (2σ) in the $M_{Z'}$-$g_{Z'}$ plane for the $B - L$ (a) and $B_y + L_\mu + L_\tau$ (b) models.

are three corresponding red dashed lines in figure 4. The lowest one represents the upper boundary of the 2σ allowed region where the contribution of the Z' boson to $Q^V_{\ell,\mathrm{SM+V}}$ is small, similarly to the blue-dashed line below and the black line further below that correspond to the CsI fit and the combined fit, respectively. The two red-dashed lines above delimit the strip in which the Ar data are well-fitted $Q^V_{\ell,\mathrm{SM+V}} \simeq -Q^V_{\mathrm{SM}}$, as discussed above for the combined fit. However, since the Ar data are less constraining, the strip is wider than those obtained from the CsI and combined analyses and it extends to small values of $M_{Z'}$.

In figure 4 we compared the limits obtained from the COHERENT CEνNS data with those of non-CEνNS experiments and those of the CONNIE reactor CEνNS experiment [154]. Figure 4 shows also the $(g-2)_\mu$ 2σ allowed band which can explain the anomalous magnetic moment of the muon in this model [56, 68] (see appendix B). One can see that the explanation of the $(g-2)_\mu$ anomaly with the universal model is excluded by the combination of the non-CEνNS exclusion limits in figure 4, by the CONNIE CEνNS bounds alone, and by the COHERENT CEνNS limits alone, which confirm and extend the CONNIE CEνNS bounds. Moreover, the COHERENT CEνNS limits extend the total exclusion region by covering a previously not-excluded area for 20 MeV $\lesssim M_{Z'} \lesssim$ 200 MeV and $2 \times 10^{-5} \lesssim g_{Z'} \lesssim 10^{-4}$. The new COHERENT CE$\nu$NS limits are consistent with those obtained in ref. [26] using the first COHERENT CsI data and slightly extend the COHERENT CEνNS exclusion region.

4.2 $B - L$ model

The gauged $B - L$ model is the most popular Z' model (see, e.g., the reviews in refs. [69, 72, 73]) and its effects in CEνNS have been studied in refs. [25, 26, 71, 104, 113] using

JHEP05(2022)109

previous COHERENT data. Figure 5a shows the 2σ limits that we obtained from the COHERENT Ar and CsI data, compared with the limits obtained from other experiments and the $(g-2)_\mu$ 2σ allowed band in this model. One can see that the bounds obtained by experiments using only leptonic probes are the same as those for the universal model in figure 4, because of the same magnitudes of the lepton charges (see table 1). The coupling $g_{Z'}$ is well constrained by the accelerator experiments for large values of $M_{Z'}$ and fixed target experiments for small values of $M_{Z'}$. Note also that the allowed region for $(g-2)_\mu$ is the same as that in the universal model, because the magnetic moment of the muon is not dependent on the couplings of quarks.

On the other hand, the CEνNS bounds are different from the universal model, because the Z' contribution to $Q^V_{\mu,\mathrm{SM+V}}$ is negative and adds to the negative SM contribution. Therefore, in figure 5a there are only the upper bounds shown by the blue-dashed, red-dashed, and black-solid lines that we obtained from the CsI, Ar, and combined analyses, respectively. These limits have the same behaviour as the corresponding ones discussed in subsection 4.1 for the universal model, but are weaker because the quark charges are smaller by a factor of 3, as shown in table 1. The numerical values of the limits for small and large values of $M_{Z'}$ are given in table 2.

Figure 5a shows that, as in the universal model, the COHERENT CEνNS limit confirms the exclusion of the explanation of the $(g-2)_\mu$ anomaly with the $B-L$ model and extends the total exclusion region of non-CEνNS experiments by covering a previously not-excluded area for 10 MeV $\lesssim M_{Z'} \lesssim$ 200 MeV and $5\times10^{-5} \lesssim g_{Z'} \lesssim 3\times10^{-4}$. Also in this case, the new COHERENT CEνNS limits are consistent with those obtained in ref. [26] using the first COHERENT CsI data and slightly extend the COHERENT CEνNS exclusion region.

4.3 $B_y + L_\mu + L_\tau$ model

The 2σ limits that we obtained for $g_{Z'}$ and $M_{Z'}$ in the $B_y + L_\mu + L_\tau$ model [113, 114] from the COHERENT Ar and CsI data are shown in figure 5b. One can see that the result of the analyses of the CsI and combined Ar and CsI data are qualitatively similar to those discusses in subsection 4.1 for the universal model: there is a lower curve that represents the upper boundary of the 2σ allowed region where the contribution of the Z' boson to $Q^V_{\ell,\mathrm{SM+V}}$ is small and a thin allowed strip where $Q^V_{\ell,\mathrm{SM+V}} \simeq -Q^V_{\mathrm{SM}}$, leading to a degeneracy with the SM cross section that can fit well the data. Neglecting the form factors and the small proton SM contribution, one can find that in the case of the $B_y + L_\mu + L_\tau$ model the thin allowed strip lies at

$$(g_{Z'}^{B_y+L_\mu+L_\tau})_{\mathrm{strip}} \simeq \sqrt{\frac{N}{A}\sqrt{2}G_F M_{Z'}^2} \simeq 3.1\times10^{-3}\,\frac{M_{Z'}}{\mathrm{GeV}}. \tag{4.3}$$

Under the same approximations, one can find that the cancellation between the SM and Z' contributions to $Q^V_{\ell,\mathrm{SM+V}}$ occurs in the parameter space between the lower upper bound curve and the thin allowed strip for

$$(g_{Z'}^{B_y+L_\mu+L_\tau})_{\mathrm{canc}} \simeq \sqrt{\frac{N}{A}\frac{\sqrt{2}G_F M_{Z'}^2}{2}} \simeq 2.2\times10^{-3}\,\frac{M_{Z'}}{\mathrm{GeV}}. \tag{4.4}$$

JHEP05(2022)109

Since the Ar data are less constraining than the CsI data, the 2σ allowed region in figure 5b is that below the upper red-dashed line, with the exception of the excluded thin strip that corresponds to the cancellation condition, see eq. (4.4).

Figure 5b shows also the LHCb [150] limits on $g_{Z'}$ in the $B_y + L_\mu + L_\tau$ model and the $(g-2)_\mu$ 2σ allowed band. One can see that the LHCb bounds exclude the $(g-2)_\mu$ allowed band only for some ranges of values of $M_{Z'}$ above about 200 MeV. On the other hand, the bounds that we obtained from the analysis of the COHERENT CEνNS data exclude all the $(g-2)_\mu$ allowed band, leading to the rejection of the explanation of the $(g-2)_\mu$ anomaly with the $B_y + L_\mu + L_\tau$ model.

4.4 $B - 3L_e$ model

Figure 6a shows the 2σ limits that we obtained from the COHERENT Ar and CsI data in the $B-3L_e$ model [102, 104, 113, 115], compared with the limits obtained from non-CEνNS experiments, which are quite strong, because there are many experiments that probe the interactions of electrons and their coupling with the Z' boson in this model is three times stronger than that in the $B - L$ model. Strict limits are especially derived from e^+e^- collider data.

Note that in figure 6a obviously there is no $(g-2)_\mu$ allowed region, because in this model the Z' boson does not interact with muonic flavor. On the other hand, there is the $(g-2)_e$ obtained from the measurement of the magnetic moment of the electron [155, 156] which is compatible with the prediction at 1.6σ level taking into account the recent determination of the fine structure constant [157].

These limits that we obtained from the combined analysis of the COHERENT CsI and Ar CEνNS data have the same behaviour as the corresponding ones for the $B - L$ model. They have also similar magnitudes, because the lack of interaction with Z' of the dominant ν_μ and $\bar{\nu}_\mu$ fluxes is compensated by the threefold increase of the ν_e coupling. The numerical values of the limits for small and large values of $M_{Z'}$ are given in table 2.

Figure 6a shows that the COHERENT CsI and Ar CEνNS data allow us to extend the total exclusion region of non-CEνNS by covering a previously not-excluded area for 10 MeV $\lesssim M_{Z'} \lesssim$ 100 MeV and $5 \times 10^{-5} \lesssim g_{Z'} \lesssim 2 \times 10^{-4}$.

4.5 $B - 3L_\mu$ model

Figure 6b shows the 2σ limits that we obtained from the COHERENT Ar and CsI data in the $B-3L_\mu$ model [104, 113, 115], compared with the limits obtained from the LHCb [150] experiment ($Z' \to \mu^+\mu^-$), which exist and are relatively strong only for $M_{Z'} \gtrsim 200$ MeV. The figure shows also the $(g-2)_\mu$ 2σ allowed band in this model, which is not excluded by the LHCb bounds for $M_{Z'} \lesssim 200$ MeV, but it is completely excluded by the bounds that we obtained from the analysis of the COHERENT CEνNS data.

4.6 $B - 2L_e - L_\mu$ model

In this model [104] both ν_e and ν_μ interact with the Z' boson as in the $B - L$ model, but the interaction of the subdominant ν_e flux is twice stronger. Therefore the bounds

JHEP05(2022)109

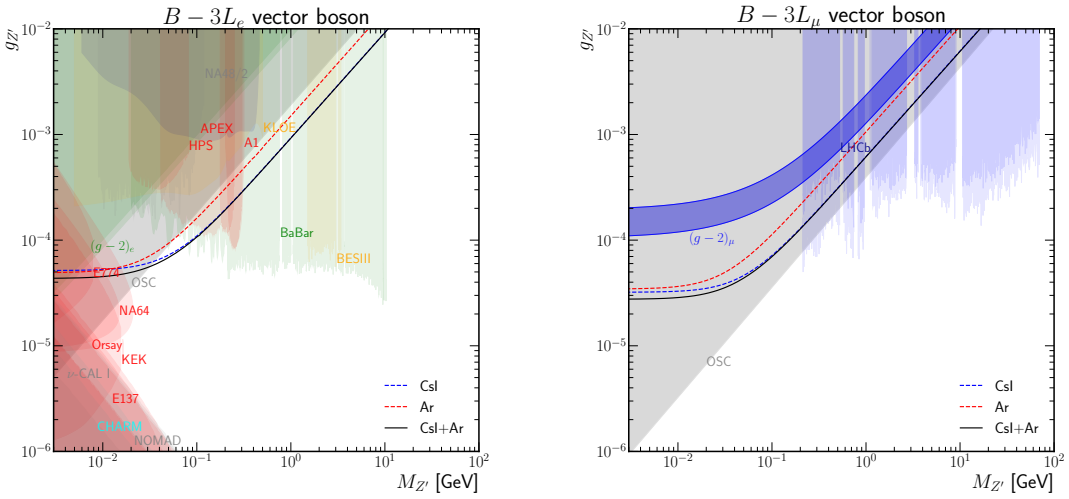

(a) **(b)**

Figure 6. Excluded regions (2σ) in the $M_{Z'}$-$g_{Z'}$ plane for the $B-3L_e$ (a) and $B-3L_\mu$ (b) models.

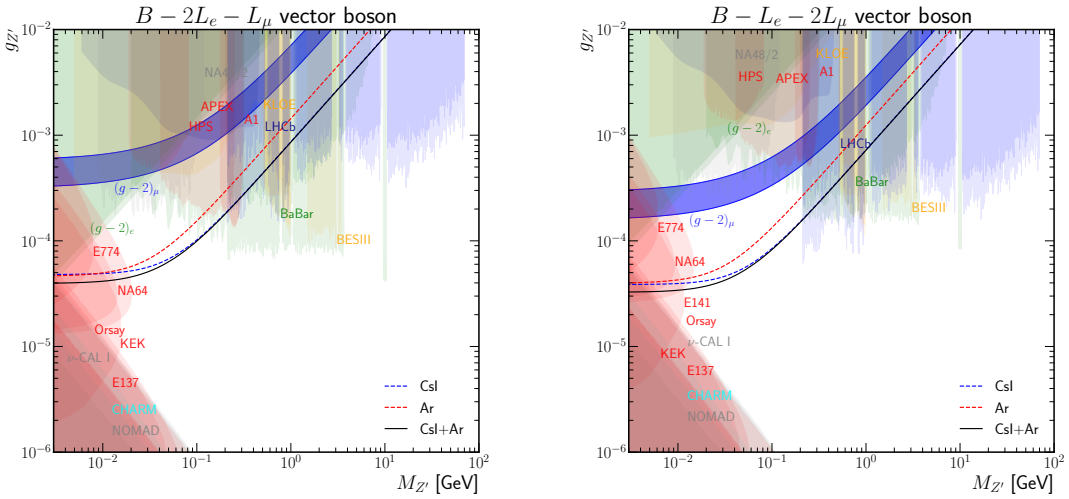

(a) **(b)**

Figure 7. Excluded regions (2σ) in the $M_{Z'}$-$g_{Z'}$ plane for the $B-2L_e-L_\mu$ (a) and $B-L_e-2L_\mu$ (b) models.

JHEP05(2022)109

that we obtained from the analyses of the COHERENT CEνNS data, shown in figure 7a are similar and slightly stronger than those in the $B-L$ model (see also table 2). From figure 7a one can also see that the $(g-2)_\mu$ 2σ allowed band in this model is excluded by the total exclusion limits of non-CEνNS experiments. The analysis of the COHERENT CsI and Ar CEνNS data allows us to extend the total exclusion region of non-CEνNS experiments by covering a previously not-excluded area for 10 MeV $\lesssim M_{Z'} \lesssim$ 100 MeV and $5\times10^{-5} \lesssim g_{Z'} \lesssim 2\times10^{-4}$.

4.7 $B-L_e-2L_\mu$ model

The phenomenology of this model [104] is similar to that of the $B-2L_e-L_\mu$ model, with the difference that the bounds obtained from the COHERENT CEνNS data are stronger, because the interactions with the Z' boson of the dominant ν_μ and $\bar{\nu}_\mu$ fluxes are twice stronger than those of the subdominant ν_e flux, as one can see from figure 7b and table 2. One can also see from figure 7b that the limits from non-CEνNS are weaker than those in figure 7a for the $B-2L_e-L_\mu$ model, whereas those obtained in ν_μ experiments are stronger. As a result, the $(g-2)_\mu$ 2σ allowed band in this model is not completely excluded by the results of non-CEνNS experiments, but it is completely excluded by the bounds that we obtained from the analysis of the COHERENT CsI and Ar CEνNS data. Moreover, we extend the total exclusion region of non-CEνNS experiments by covering a previously not-excluded area for 10 MeV $\lesssim M_{Z'} \lesssim$ 200 MeV and $3\times10^{-5} \lesssim g_{Z'} \lesssim 3\times10^{-4}$.

4.8 L_e-L_μ model

Figure 8a shows the 2σ limits that we obtained from the COHERENT Ar and CsI data in the L_e-L_μ model [76, 113, 116]. As for all the $L_\alpha-L_\beta$ models the constraints that we can obtain from CEνNS data are weaker than those in the previous models, because the interaction with quarks occurs only at loop level, and hence it is weaker. This is also shown by the values in table 2 where one can see that the bounds in the $L_\alpha-L_\beta$ are more than one order of magnitude weaker than those corresponding to the models that we considered in the previous subsections. Moreover, in spite of the fact that all the neutrino fluxes (ν_e, ν_μ, and $\bar{\nu}_\mu$) interact with the Z' boson in this model, the Z' contribution to the CEνNS event rate is suppressed by the opposite signs of the ν_e and ν_μ contributions to $Q^V_{\mu,\mathrm{SM+V}}$ explained at the end of subsection 3.1 and illustrated by the red-dashed curves in figures 1c and 1d.

One can see from figure 8a that the bounds obtained from the current COHERENT CEνNS data are not competitive with those obtained from non-CEνNS experiments and do not contribute to the exclusion of the $(g-2)_\mu$ 2σ allowed band in this model. Let us note that most of this band is excluded by non-CEνNS experiments, but there is a small non-excluded part at $M_{Z'} \approx 20-30$ MeV and $g_{Z'} \approx (4-7)\times10^{-4}$.

4.9 L_e-L_τ model

Since in the L_e-L_τ model [76, 113, 116] the dominant ν_μ in the COHERENT experiment is not interacting with the Z' boson, the bounds on the parameters of the model are rather weak. From figure 8b and table 2, one can see that they are comparable with the bounds in the L_e-L_μ model, with the difference that there is an allowed diagonal strip

JHEP05(2022)109

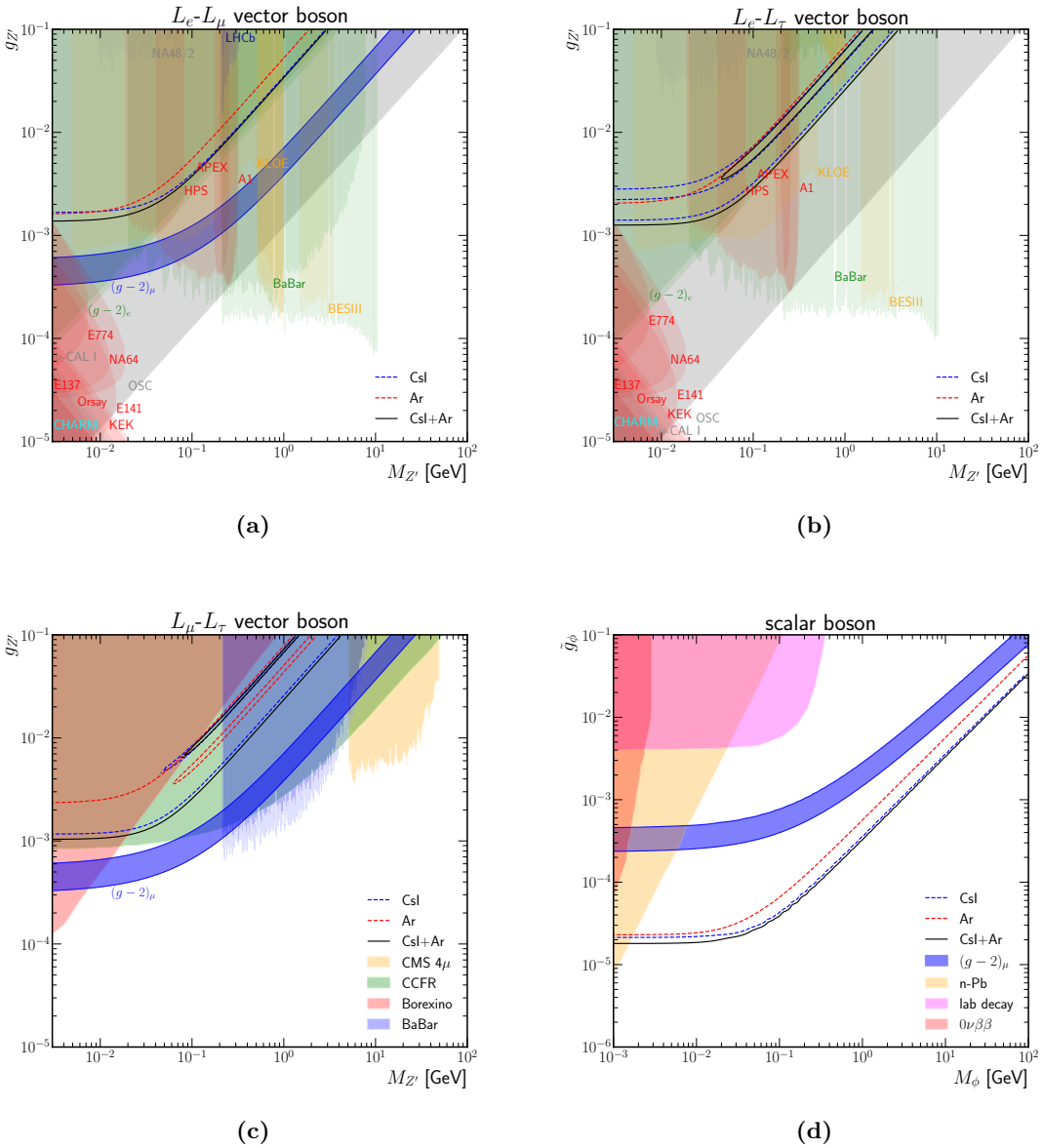

Figure 8. Excluded regions (2σ) in the mass-coupling plane for the $L_e - L_\tau$ (a), $L_e - L_\mu$ (b), $L_\mu - L_\tau$ (c), and scalar (d) models.

for $M_{Z'} \gtrsim 50$ MeV. This occurs in the $L_e - L_\tau$ model because of the different signs of the SM and Z' contributions to $Q^V_{\ell,\mathrm{SM+V}}$ discussed in subsection 3.1. The allowed strip is the region of the parameters where $Q^V_{\ell,\mathrm{SM+V}} \simeq -Q^V_{\mathrm{SM}}$, leading to a degeneracy with the SM cross section, as for the similar strips in figure 4 for the universal model and figure 5b for the $B_y + L_\mu + L_\tau$ model. Neglecting the form factors and the small proton SM contribution,

JHEP05(2022)109

this degeneracy occurs for

$$(g_{Z'}^{L_e-L_\tau})_{\rm strip} \approx \sqrt{\frac{N}{Z}\frac{\pi G_F M_{Z'}^2}{\sqrt{2}\alpha_{\rm EM}\varepsilon_{\tau e}}} \approx 6\times 10^{-2}\,\frac{M_{Z'}}{\rm GeV}, \tag{4.5}$$

where we considered $N/Z \approx 1.3$ and $\varepsilon_{\tau e} \approx 1.5$. One can see from figure 8b that the allowed diagonal strip lies along the line given by eq. (4.5).

The non-CEνNS bounds in figure 8b are the same as the bounds in figure 8a that have been obtained with electron-interaction experiments, including that from $(g-2)_e$ value [155–157] that we already mentioned above in subsection 4.4 for the $B-3L_e$ model. From figure 8b one can see that in the $L_e - L_\tau$ model the bounds obtained from the current COHERENT CEνNS data are not competitive with those obtained from non-CEνNS experiments and the non-CEνNS experiments exclude the CEνNS allowed diagonal strip discussed above.

4.10 $L_\mu - L_\tau$ model

Figure 8c shows the 2σ limits that we obtained from the COHERENT Ar and CsI data in the popular $L_\mu - L_\tau$ model [26, 28, 59, 71, 76, 78, 79, 117]. From figure 8c and the values in table 2, one can see that the bounds obtained in this model from the COHERENT CEνNS data are the strongest among the $L_\alpha - L_\beta$ models. This is due to the interaction with the Z' boson of the dominant ν_μ and $\bar{\nu}_\mu$ fluxes that is not suppressed by the opposite contribution of the ν_e flux as in the $L_e - L_\mu$ model.

From figure 8c, one can also see that there is an allowed diagonal strip that is the region of the parameters where $Q^V_{\ell,\rm SM+V} \simeq -Q^V_{\rm SM}$, which is due to the different signs of the SM and Z' contributions to $Q^V_{\ell,\rm SM+V}$, as discussed above for other models. Since $\varepsilon_{\tau\mu} \simeq \ln(m_\tau^2/m_\mu^2)/6$, as discussed in subsection 3.1, the allowed diagonal strip corresponds to

$$(g_{Z'}^{L_\mu-L_\tau})_{\rm strip} \approx \sqrt{\frac{N}{Z}\frac{6\pi G_F M_{Z'}^2}{\sqrt{2}\alpha_{\rm EM}\ln(m_\tau^2/m_\mu^2)}} \approx 7\times 10^{-2}\,\frac{M_{Z'}}{\rm GeV}, \tag{4.6}$$

where we considered $N/Z \approx 1.3$

One can see form figure 8c that in the $L_\mu - L_\tau$ model there are several non-CEνNS constraints whose combination is more stringent than those given by the current COHERENT CEνNS data: CMS [158] ($Z \to Z'\mu\mu \to 4\mu$), BaBar [159] ($e^+e^- \to Z'\mu\mu \to 4\mu$), CCFR [160, 161] (neutrino trident production), and Borexino [117, 162, 163] (Z'-mediated solar neutrino interactions). These non-CEνNS constraints exclude the allowed diagonal strip corresponding to eq. (4.6). On the other hand, they do not completely exclude the $(g-2)_\mu$ 2σ allowed band in this model, that is shown in figure 8c. One can see that the part of this band for 10 MeV $\lesssim M_{Z'} \lesssim$ 200 MeV and $3\times10^{-4} \lesssim g_{Z'} \lesssim 10^{-3}$ eludes the exclusions.

4.11 Scalar model

Figure 8d shows the 2σ limits that we obtained from the COHERENT Ar and CsI data in the scalar boson mediator model described in subsection 3.2. The figure shows also the $(g-2)_\mu$ 2σ allowed band in this model and the constraints obtained from the measurement

JHEP05(2022)109

of neutrons scattering on a ^{208}Pb target [164–166], the measurement of τ, mesons, and Z decays [167–172], and double-beta decay experiments [167, 173–175] (see also the summary in ref. [126]).

One can see from figure 8d that the COHERENT CEνNS constraints are much more stringent than the non-CEνNS bounds for $M_\phi \gtrsim 2$ MeV and they exclude the explanation of the $(g-2)_\mu$ anomaly in the scalar boson mediator model.

5 Conclusions

In this paper we analyzed the recent CEνNS data obtained by the COHERENT Collaboration with the CsI and Ar detectors and we derived constraints on the coupling and mass of a non-standard light vector or scalar boson mediator considering several models that have been studied in the literature. We presented the results obtained from the separate analyses of the CsI and Ar data and those obtained from the combined analysis of the two datasets.

We considered several models with a light vector boson Z': the anomalous model with universal coupling of the Z' vector boson with all SM fermions (assuming that the quantum anomalies are canceled by the contributions of the non-standard fermions of an extended full theory), several anomaly-free models with gauged U(1)$'$ symmetries, as the popular $B-L$ symmetry, in which the Z' vector boson couples directly to quarks and leptons, and the anomaly-free models with gauged L_e-L_μ, L_e-L_τ, and $L_\mu-L_\tau$ symmetries, in which the Z' vector boson couples directly to the involved lepton flavors and indirectly to nucleons at the one-loop level.

We compared the constraints obtained from the COHERENT CsI and Ar CEνNS data with those obtained from several non-CEνNS experiments. We showed that the COHERENT CEνNS data allow us to extend the excluded regions of the parameters in the models in which the Z' vector boson couples directly to quarks and in the universal scalar mediator model. In particular, the total excluded region is extended to smaller values of the coupling constant $g_{Z'}$ for 10 MeV $\lesssim M_{Z'} \lesssim$ 100 MeV in the universal, $B-L$, $B-3L_e$, $B-2L_e-L_\mu$, and $B-L_e-2L_\mu$ models. The regions in the $M_{Z'}$-$g_{Z'}$ plane that are excluded by non-CEνNS experiments for the $B_y+L_\mu+L_\tau$ and $B-3L_\mu$ models are limited to $M_{Z'} \gtrsim 200$ MeV. Therefore, for these models the COHERENT CEνNS data allow us to obtain a large extension of the total excluded region for $M_{Z'} \lesssim 200$ MeV.

The models in which the Z' couples to muons can explain the $(g-2)_\mu$ anomaly [29, 55, 56], and the allowed band in the $M_{Z'}$-$g_{Z'}$ plane is tested by non-CEνNS experiments, as shown in figures 4, 5, 6, and 7. The results of our analysis of the COHERENT CEνNS data exclude the explanation of the $(g-2)_\mu$ anomaly in the models in which the Z' vector boson couples directly to quarks by confirming the excluded regions of non-CEνNS experiments and extending the coverage of the $(g-2)_\mu$ allowed band for the $B_y+L_\mu+L_\tau$, $B-3L_\mu$, and $B-L_e-2L_\mu$ models.

The constraints that we obtained for the L_e-L_μ, L_e-L_τ, and $L_\mu-L_\tau$ are less stringent because the one-loop interactions of the Z' vector boson with the nucleons is weaker than the direct interaction. For these models the current COHERENT CEνNS data allow us to

JHEP05(2022)109

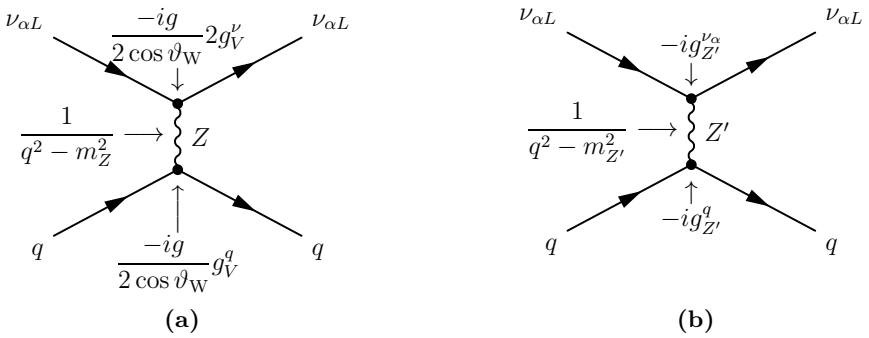

Figure 9. Feynman diagrams describing (a) the vector part of the Standard Model neutral-current interaction and (b) the Z' vector interaction of left-handed neutrinos with quarks.

confirm the exclusion of part of the parameter space that is already covered by non-CEνNS experiments, but cannot probe the $(g-2)_\mu$ allowed band in the $L_e - L_\mu$ and $L_\mu - L_\tau$ models.

We finally considered CEνNS interactions mediated by a light scalar boson ϕ assuming for simplicity a universal coupling with the quarks and neutrinos involved in the CEνNS processes measured in the COHERENT experiment. We obtained the strong constraints on the mass M_ϕ and coupling of the scalar boson shown in figure 8d that greatly extend the region excluded by non-CEνNS experiments and rejects the explanation of the $(g-2)_\mu$ anomaly in this model.

Acknowledgments

We would like to thank A. Konovalov and D. Pershey for the useful information provided for the analysis of the COHERENT data. The work of C. Giunti and C.A. Ternes is supported by the research grant "The Dark Universe: A Synergic Multimessenger Approach" number 2017X7X85K under the program PRIN 2017 funded by the Ministero dell'Istruzione, Università e della Ricerca (MIUR). The work of Y.F. Li and Y.Y. Zhang is supported by the National Natural Science Foundation of China under Grant No. 12075255, 12075254 and No. 11835013, by the Key Research Program of the Chinese Academy of Sciences under Grant No. XDPB15. Y.F. Li is also grateful for the support by the CAS Center for Excellence in Particle Physics (CCEPP). The work of Y.Y. Zhang is also supported by China Postdoctoral Science Foundation under Grant No. 2021T140669.

A Z' coupling

There is some confusion on the value of the coefficient of the contribution of a new Z' vector boson mediator in eq. (3.7) that is obtained assuming the interaction Lagrangian in eq. (3.6). For example, in refs. [6, 12, 15, 16, 99, 100] the coefficient is half of that in eq. (3.7). On the other hand, the coefficient in refs. [14, 19, 25, 26, 70, 71, 101–105] agrees with that in eq. (3.7). In this appendix we prove that the coefficient in eq. (3.7) is the right one.

JHEP05(2022)109

Let us start by considering the relevant vector part of the Standard Model neutral-current weak interaction Lagrangian (see, e.g., refs. [85, 110])

$$\mathcal{L}_Z^V = -\frac{g}{2\cos\vartheta_{\rm W}} Z_\mu \left[2g_V^\nu \sum_{\ell=e,\mu,\tau} \overline{\nu_{\ell L}}\gamma^\mu \nu_{\ell L} + \sum_{q=u,d} g_V^q\, \overline{q}\gamma^\mu q \right], \tag{A.1}$$

with the tree-level couplings

$$g_V^\nu = \frac{1}{2}, \quad g_V^u = \frac{1}{2} - \frac{4}{3}\sin^2\vartheta_{\rm W}, \quad \text{and} \quad g_V^d = -\frac{1}{2} + \frac{2}{3}\sin^2\vartheta_{\rm W}. \tag{A.2}$$

Confronting eq. (A.1) with the Lagrangian (3.6), one can see that the Z' vector interaction of left-handed neutrinos with quarks is obtained from the vector part of the Standard Model neutral-current interaction with the substitutions

$$\frac{g}{2\cos\vartheta_{\rm W}} 2g_V^\nu \to g_{Z'}^{\nu_\ell V}, \quad \frac{g}{2\cos\vartheta_{\rm W}} g_V^q \to g_{Z'}^{qV}, \quad \text{and} \quad m_Z \to m_{Z'}. \tag{A.3}$$

This correspondence is shown in figure 9, where we depicted the two Feynman diagrams that describe the neutrino-quarks interactions that contribute to CEνNS at tree level. The total amplitude is given by the sum of the two diagrams

$$A \propto \frac{g^2}{4\cos^2\vartheta_{\rm W}} \frac{2g_V^\nu g_V^q}{q^2 - m_Z^2} + \frac{g_{Z'}^{\nu_\ell V} g_{Z'}^{qV}}{q^2 - m_{Z'}^2}. \tag{A.4}$$

Taking into account that $g_V^\nu = 1/2$ and

$$\frac{g^2}{4\cos^2\vartheta_{\rm W} m_Z^2} = \sqrt{2} G_{\rm F}, \tag{A.5}$$

for $q^2 \ll m_Z^2$ we obtain

$$A \propto g_V^q + \frac{g_{Z'}^{\nu_\ell V} g_{Z'}^{qV}}{\sqrt{2} G_{\rm F} \left(q^2 - m_{Z'}^2\right)}. \tag{A.6}$$

This relation leads to eq. (3.7), taking into account that the conservation of the vector current implies that

$$g_{Z'}^p = 2g_{Z'}^{uV} + g_{Z'}^{dV} \quad \text{and} \quad g_{Z'}^n = g_{Z'}^{uV} + 2g_{Z'}^{dV}. \tag{A.7}$$

In conclusion of this appendix, let us note that the results of the analyses in refs. [6, 12, 15, 16, 99, 100], where the Z' contribution to the weak charge in CEνNS is half of that in eq. (3.7), must be reinterpreted by rescaling their Z' coupling $g_{Z'}$ by a factor $\sqrt{2}$.

B Muon $g-2$

Recently, the Fermilab Muon $g-2$ experiment [56] confirmed the value of the muon anomalous magnetic moment $(g-2)_\mu$ that was measured in 2006 in the Muon E821 experiment at Brookhaven National Laboratory [55], leading to the combined 4.2σ deviation from the Standard Model prediction

$$\Delta a_\mu = (25.1 \pm 5.9) \times 10^{-10}, \tag{B.1}$$

JHEP05(2022)109

where $a_\mu = (g-2)_\mu/2$. This $(g-2)_\mu$ anomaly may be due to new physics beyond the SM (see the reviews in refs. [68, 176, 177]).

In theories beyond the SM, an additional neutral boson B with mass M_B, which interacts with muons with coupling g_B, contributes to the muon anomalous magnetic moment with [178]

$$\delta a_\mu^B = \frac{g_B^2}{8\pi^2} \int_0^1 dx \, \frac{Q(x)}{x^2 + (1-x)\, M_B^2/m_\mu^2} \tag{B.2}$$

where $Q(x)$ depends on the scalar or vector nature of the neutral boson B:

$$Q(x) = \begin{cases} x^2\,(2-x) & \text{(scalar)}, \\ 2x^2\,(1-x) & \text{(vector)}. \end{cases} \tag{B.3}$$

References

[1] COHERENT collaboration, *Observation of coherent elastic neutrino-nucleus scattering*, *Science* **357** (2017) 1123 [arXiv:1708.01294] [INSPIRE].

[2] COHERENT collaboration, *COHERENT collaboration data release from the first observation of coherent elastic neutrino-nucleus scattering*, arXiv:1804.09459 [INSPIRE].

[3] M. Cadeddu, C. Giunti, Y.F. Li and Y.Y. Zhang, *Average CsI neutron density distribution from COHERENT data*, *Phys. Rev. Lett.* **120** (2018) 072501 [arXiv:1710.02730] [INSPIRE].

[4] D.K. Papoulias, T.S. Kosmas, R. Sahu, V.K.B. Kota and M. Hota, *Constraining nuclear physics parameters with current and future COHERENT data*, *Phys. Lett. B* **800** (2020) 135133 [arXiv:1903.03722] [INSPIRE].

[5] P. Coloma, M.C. Gonzalez-Garcia, M. Maltoni and T. Schwetz, *COHERENT enlightenment of the neutrino dark side*, *Phys. Rev. D* **96** (2017) 115007 [arXiv:1708.02899] [INSPIRE].

[6] J. Liao and D. Marfatia, *COHERENT constraints on nonstandard neutrino interactions*, *Phys. Lett. B* **775** (2017) 54 [arXiv:1708.04255] [INSPIRE].

[7] M. Lindner, W. Rodejohann and X.-J. Xu, *Coherent neutrino-nucleus scattering and new neutrino interactions*, *JHEP* **03** (2017) 097 [arXiv:1612.04150] [INSPIRE].

[8] C. Giunti, *General COHERENT constraints on neutrino nonstandard interactions*, *Phys. Rev. D* **101** (2020) 035039 [arXiv:1909.00466] [INSPIRE].

[9] P.B. Denton, Y. Farzan and I.M. Shoemaker, *Testing large non-standard neutrino interactions with arbitrary mediator mass after COHERENT data*, *JHEP* **07** (2018) 037 [arXiv:1804.03660] [INSPIRE].

[10] D. Aristizabal Sierra, V. De Romeri and N. Rojas, *COHERENT analysis of neutrino generalized interactions*, *Phys. Rev. D* **98** (2018) 075018 [arXiv:1806.07424] [INSPIRE].

[11] M. Cadeddu, C. Giunti, K.A. Kouzakov, Y.-F. Li, Y.-Y. Zhang and A.I. Studenikin, *Neutrino charge radii from coherent elastic neutrino-nucleus scattering*, *Phys. Rev. D* **98** (2018) 113010 [*Erratum ibid.* **101** (2020) 059902] [arXiv:1810.05606] [INSPIRE].

JHEP05(2022)109

[12] D.K. Papoulias and T.S. Kosmas, *COHERENT constraints to conventional and exotic neutrino physics*, *Phys. Rev. D* **97** (2018) 033003 [arXiv:1711.09773] [INSPIRE].

[13] M. Cadeddu, F. Dordei, C. Giunti, Y.F. Li and Y.Y. Zhang, *Neutrino, electroweak, and nuclear physics from COHERENT elastic neutrino-nucleus scattering with refined quenching factor*, *Phys. Rev. D* **101** (2020) 033004 [arXiv:1908.06045] [INSPIRE].

[14] D.K. Papoulias, *COHERENT constraints after the COHERENT-2020 quenching factor measurement*, *Phys. Rev. D* **102** (2020) 113004 [arXiv:1907.11644] [INSPIRE].

[15] A.N. Khan and W. Rodejohann, *New physics from COHERENT data with an improved quenching factor*, *Phys. Rev. D* **100** (2019) 113003 [arXiv:1907.12444] [INSPIRE].

[16] B. Dutta, S. Liao, S. Sinha and L.E. Strigari, *Searching for beyond the Standard Model physics with COHERENT energy and timing data*, *Phys. Rev. Lett.* **123** (2019) 061801 [arXiv:1903.10666] [INSPIRE].

[17] M. Cadeddu and F. Dordei, *Reinterpreting the weak mixing angle from atomic parity violation in view of the Cs neutron rms radius measurement from COHERENT*, *Phys. Rev. D* **99** (2019) 033010 [arXiv:1808.10202] [INSPIRE].

[18] B. Dutta, D. Kim, S. Liao, J.-C. Park, S. Shin and L.E. Strigari, *Dark matter signals from timing spectra at neutrino experiments*, *Phys. Rev. Lett.* **124** (2020) 121802 [arXiv:1906.10745] [INSPIRE].

[19] M. Abdullah, J.B. Dent, B. Dutta, G.L. Kane, S. Liao and L.E. Strigari, *Coherent elastic neutrino nucleus scattering as a probe of a Z' through kinetic and mass mixing effects*, *Phys. Rev. D* **98** (2018) 015005 [arXiv:1803.01224] [INSPIRE].

[20] S.-F. Ge and I.M. Shoemaker, *Constraining photon portal dark matter with Texono and coherent data*, *JHEP* **11** (2018) 066 [arXiv:1710.10889] [INSPIRE].

[21] COHERENT collaboration, *First measurement of coherent elastic neutrino-nucleus scattering on argon*, *Phys. Rev. Lett.* **126** (2021) 012002 [arXiv:2003.10630] [INSPIRE].

[22] COHERENT collaboration, *COHERENT collaboration data release from the first detection of coherent elastic neutrino-nucleus scattering on argon*, arXiv:2006.12659 [INSPIRE].

[23] D. Akimov et al., *Measurement of the coherent elastic neutrino-nucleus scattering cross section on CsI by COHERENT*, arXiv:2110.07730 [INSPIRE].

[24] M. Cadeddu, F. Dordei, C. Giunti, Y.F. Li, E. Picciau and Y.Y. Zhang, *Physics results from the first COHERENT observation of coherent elastic neutrino-nucleus scattering in argon and their combination with cesium-iodide data*, *Phys. Rev. D* **102** (2020) 015030 [arXiv:2005.01645] [INSPIRE].

[25] O.G. Miranda, D.K. Papoulias, G. Sanchez Garcia, O. Sanders, M. Tórtola and J.W.F. Valle, *Implications of the first detection of coherent elastic neutrino-nucleus scattering (CEνNS) with liquid argon*, *JHEP* **05** (2020) 130 [*Erratum ibid.* **01** (2021) 067] [arXiv:2003.12050] [INSPIRE].

[26] M. Cadeddu et al., *Constraints on light vector mediators through coherent elastic neutrino nucleus scattering data from COHERENT*, *JHEP* **01** (2021) 116 [arXiv:2008.05022] [INSPIRE].

[27] M. Cadeddu et al., *New insights into nuclear physics and weak mixing angle using electroweak probes*, *Phys. Rev. C* **104** (2021) 065502 [arXiv:2102.06153] [INSPIRE].

JHEP05(2022)109

[28] H. Banerjee, B. Dutta and S. Roy, *Probing $L_\mu - L_\tau$ models with CEνNS: a new look at the combined COHERENT CsI and Ar data*, *Phys. Rev. D* **104** (2021) 015015 [arXiv:2103.10196] [INSPIRE].

[29] T. Aoyama et al., *The anomalous magnetic moment of the muon in the Standard Model*, *Phys. Rept.* **887** (2020) 1 [arXiv:2006.04822] [INSPIRE].

[30] T. Aoyama, M. Hayakawa, T. Kinoshita and M. Nio, *Complete tenth-order QED contribution to the muon $g-2$*, *Phys. Rev. Lett.* **109** (2012) 111808 [arXiv:1205.5370] [INSPIRE].

[31] T. Aoyama, T. Kinoshita and M. Nio, *Theory of the anomalous magnetic moment of the electron*, *Atoms* **7** (2019) 28 [INSPIRE].

[32] A. Czarnecki, W.J. Marciano and A. Vainshtein, *Refinements in electroweak contributions to the muon anomalous magnetic moment*, *Phys. Rev. D* **67** (2003) 073006 [*Erratum ibid.* **73** (2006) 119901] [hep-ph/0212229] [INSPIRE].

[33] C. Gnendiger, D. Stöckinger and H. Stöckinger-Kim, *The electroweak contributions to $(g-2)_\mu$ after the Higgs boson mass measurement*, *Phys. Rev. D* **88** (2013) 053005 [arXiv:1306.5546] [INSPIRE].

[34] M. Davier, A. Hoecker, B. Malaescu and Z. Zhang, *Reevaluation of the hadronic vacuum polarisation contributions to the Standard Model predictions of the muon $g-2$ and $\alpha(m_Z^2)$ using newest hadronic cross-section data*, *Eur. Phys. J. C* **77** (2017) 827 [arXiv:1706.09436] [INSPIRE].

[35] A. Keshavarzi, D. Nomura and T. Teubner, *Muon $g-2$ and $\alpha(M_Z^2)$: a new data-based analysis*, *Phys. Rev. D* **97** (2018) 114025 [arXiv:1802.02995] [INSPIRE].

[36] G. Colangelo, M. Hoferichter and P. Stoffer, *Two-pion contribution to hadronic vacuum polarization*, *JHEP* **02** (2019) 006 [arXiv:1810.00007] [INSPIRE].

[37] M. Hoferichter, B.-L. Hoid and B. Kubis, *Three-pion contribution to hadronic vacuum polarization*, *JHEP* **08** (2019) 137 [arXiv:1907.01556] [INSPIRE].

[38] M. Davier, A. Hoecker, B. Malaescu and Z. Zhang, *A new evaluation of the hadronic vacuum polarisation contributions to the muon anomalous magnetic moment and to $\alpha(m_Z^2)$*, *Eur. Phys. J. C* **80** (2020) 241 [*Erratum ibid.* **80** (2020) 410] [arXiv:1908.00921] [INSPIRE].

[39] A. Keshavarzi, D. Nomura and T. Teubner, *$g-2$ of charged leptons, $\alpha(M_Z^2)$, and the hyperfine splitting of muonium*, *Phys. Rev. D* **101** (2020) 014029 [arXiv:1911.00367] [INSPIRE].

[40] K. Melnikov and A. Vainshtein, *Hadronic light-by-light scattering contribution to the muon anomalous magnetic moment revisited*, *Phys. Rev. D* **70** (2004) 113006 [hep-ph/0312226] [INSPIRE].

[41] P. Masjuan and P. Sanchez-Puertas, *Pseudoscalar-pole contribution to the $(g_\mu - 2)$: a rational approach*, *Phys. Rev. D* **95** (2017) 054026 [arXiv:1701.05829] [INSPIRE].

[42] G. Colangelo, M. Hoferichter, M. Procura and P. Stoffer, *Dispersion relation for hadronic light-by-light scattering: two-pion contributions*, *JHEP* **04** (2017) 161 [arXiv:1702.07347] [INSPIRE].

JHEP05(2022)109

[43] M. Hoferichter, B.-L. Hoid, B. Kubis, S. Leupold and S.P. Schneider, *Dispersion relation for hadronic light-by-light scattering: pion pole*, *JHEP* **10** (2018) 141 [arXiv:1808.04823] [INSPIRE].

[44] A. Gérardin, H.B. Meyer and A. Nyffeler, *Lattice calculation of the pion transition form factor with $N_f = 2 + 1$ Wilson quarks*, *Phys. Rev. D* **100** (2019) 034520 [arXiv:1903.09471] [INSPIRE].

[45] J. Bijnens, N. Hermansson-Truedsson and A. Rodríguez-Sánchez, *Short-distance constraints for the HLbL contribution to the muon anomalous magnetic moment*, *Phys. Lett. B* **798** (2019) 134994 [arXiv:1908.03331] [INSPIRE].

[46] G. Colangelo, F. Hagelstein, M. Hoferichter, L. Laub and P. Stoffer, *Longitudinal short-distance constraints for the hadronic light-by-light contribution to $(g-2)_\mu$ with large-N_c Regge models*, *JHEP* **03** (2020) 101 [arXiv:1910.13432] [INSPIRE].

[47] V. Pauk and M. Vanderhaeghen, *Single meson contributions to the muon's anomalous magnetic moment*, *Eur. Phys. J. C* **74** (2014) 3008 [arXiv:1401.0832] [INSPIRE].

[48] I. Danilkin and M. Vanderhaeghen, *Light-by-light scattering sum rules in light of new data*, *Phys. Rev. D* **95** (2017) 014019 [arXiv:1611.04646] [INSPIRE].

[49] F. Jegerlehner, *The anomalous magnetic moment of the muon*, *Springer Tracts Mod. Phys.* **274** (2017) 1 [INSPIRE].

[50] M. Knecht, S. Narison, A. Rabemananjara and D. Rabetiarivony, *Scalar meson contributions to a μ from hadronic light-by-light scattering*, *Phys. Lett. B* **787** (2018) 111 [arXiv:1808.03848] [INSPIRE].

[51] G. Eichmann, C.S. Fischer and R. Williams, *Kaon-box contribution to the anomalous magnetic moment of the muon*, *Phys. Rev. D* **101** (2020) 054015 [arXiv:1910.06795] [INSPIRE].

[52] P. Roig and P. Sanchez-Puertas, *Axial-vector exchange contribution to the hadronic light-by-light piece of the muon anomalous magnetic moment*, *Phys. Rev. D* **101** (2020) 074019 [arXiv:1910.02881] [INSPIRE].

[53] T. Blum et al., *Hadronic light-by-light scattering contribution to the muon anomalous magnetic moment from lattice QCD*, *Phys. Rev. Lett.* **124** (2020) 132002 [arXiv:1911.08123] [INSPIRE].

[54] G. Colangelo, M. Hoferichter, A. Nyffeler, M. Passera and P. Stoffer, *Remarks on higher-order hadronic corrections to the muon $g-2$*, *Phys. Lett. B* **735** (2014) 90 [arXiv:1403.7512] [INSPIRE].

[55] MUON G-2 collaboration, *Final report of the muon E821 anomalous magnetic moment measurement at BNL*, *Phys. Rev. D* **73** (2006) 072003 [hep-ex/0602035] [INSPIRE].

[56] MUON G-2 collaboration, *Measurement of the positive muon anomalous magnetic moment to 0.46 ppm*, *Phys. Rev. Lett.* **126** (2021) 141801 [arXiv:2104.03281] [INSPIRE].

[57] P. Athron, C. Balázs, D.H.J. Jacob, W. Kotlarski, D. Stöckinger and H. Stöckinger-Kim, *New physics explanations of a_μ in light of the FNAL muon $g-2$ measurement*, *JHEP* **09** (2021) 080 [arXiv:2104.03691] [INSPIRE].

[58] M. Lindner, M. Platscher and F.S. Queiroz, *A call for new physics: the muon anomalous magnetic moment and lepton flavor violation*, *Phys. Rept.* **731** (2018) 1 [arXiv:1610.06587] [INSPIRE].

JHEP05(2022)109

[59] S. Baek, N.G. Deshpande, X.G. He and P. Ko, *Muon anomalous $g-2$ and gauged $L_\mu - L_\tau$ models*, *Phys. Rev. D* **64** (2001) 055006 [hep-ph/0104141] [INSPIRE].

[60] E. Ma, D.P. Roy and S. Roy, *Gauged $L_\mu - L_\tau$ with large muon anomalous magnetic moment and the bimaximal mixing of neutrinos*, *Phys. Lett. B* **525** (2002) 101 [hep-ph/0110146] [INSPIRE].

[61] W. Altmannshofer, M. Carena and A. Crivellin, *$L_\mu - L_\tau$ theory of Higgs flavor violation and $(g-2)_\mu$*, *Phys. Rev. D* **94** (2016) 095026 [arXiv:1604.08221] [INSPIRE].

[62] D.W.P. Amaral, D.G. Cerdeno, A. Cheek and P. Foldenauer, *Confirming $\mathrm{U}(1)_{L_\mu - L_\tau}$ as a solution for $(g-2)_\mu$ with neutrinos*, *Eur. Phys. J. C* **81** (2021) 861 [arXiv:2104.03297] [INSPIRE].

[63] M. Cadeddu, N. Cargioli, F. Dordei, C. Giunti and E. Picciau, *Muon and electron $g-2$ and proton and cesium weak charges implications on dark Z_d models*, *Phys. Rev. D* **104** (2021) 011701 [arXiv:2104.03280] [INSPIRE].

[64] S. Zhou, *Neutrino masses, leptonic flavor mixing, and muon $(g-2)$ in the seesaw model with the $\mathrm{U}(1)_{L^\mu - L^\tau}$ gauge symmetry*, *Chin. Phys. C* **46** (2022) 011001 [arXiv:2104.06858] [INSPIRE].

[65] P. Ko, T. Nomura and H. Okada, *Muon $g-2$, $B \to K^{(*)}\mu^+\mu^-$ anomalies, and leptophilic dark matter in $\mathrm{U}(1)_{\mu-\tau}$ gauge symmetry*, arXiv:2110.10513 [INSPIRE].

[66] T. Hapitas, D. Tuckler and Y. Zhang, *General kinetic mixing in gauged $\mathrm{U}(1)_{L_\mu - L_\tau}$ model for muon $g-2$ and dark matter*, *Phys. Rev. D* **105** (2022) 016014 [arXiv:2108.12440] [INSPIRE].

[67] Y. Cheng, X.-G. He and J. Sun, *Widening the $\mathrm{U}(1)_{L_\mu - L_\tau}$ Z' mass range for resolving the muon $g-2$ anomaly*, *Phys. Lett. B* **827** (2022) 136989 [arXiv:2112.09920] [INSPIRE].

[68] F. Jegerlehner and A. Nyffeler, *The muon $g-2$*, *Phys. Rept.* **477** (2009) 1 [arXiv:0902.3360] [INSPIRE].

[69] P. Langacker, *The physics of heavy Z' gauge bosons*, *Rev. Mod. Phys.* **81** (2009) 1199 [arXiv:0801.1345] [INSPIRE].

[70] J. Billard, J. Johnston and B.J. Kavanagh, *Prospects for exploring new physics in coherent elastic neutrino-nucleus scattering*, *JCAP* **11** (2018) 016 [arXiv:1805.01798] [INSPIRE].

[71] E. Bertuzzo, G.G. di Cortona and L.M.D. Ramos, *Probing light vector mediators with coherent scattering at future facilities*, arXiv:2112.04020 [INSPIRE].

[72] R.N. Mohapatra, *From old symmetries to new symmetries: quarks, leptons and $B-L$*, *Int. J. Mod. Phys. A* **29** (2014) 1430066 [arXiv:1409.7557] [INSPIRE].

[73] S. Okada, *Z' portal dark matter in the minimal $B-L$ model*, *Adv. High Energy Phys.* **2018** (2018) 5340935 [arXiv:1803.06793] [INSPIRE].

[74] R. Foot, *New physics from electric charge quantization?*, *Mod. Phys. Lett. A* **6** (1991) 527 [INSPIRE].

[75] R. Foot, G.C. Joshi, H. Lew and R.R. Volkas, *Charge quantization in the Standard Model and some of its extensions*, *Mod. Phys. Lett. A* **5** (1990) 2721 [INSPIRE].

[76] X.G. He, G.C. Joshi, H. Lew and R.R. Volkas, *New Z' phenomenology*, *Phys. Rev. D* **43** (1991) 22 [INSPIRE].

JHEP05(2022)109

[77] R. Foot, H. Lew and R.R. Volkas, *Electric charge quantization*, *J. Phys. G* **19** (1993) 361 [*Erratum ibid.* **19** (1993) 1067] [hep-ph/9209259] [INSPIRE].

[78] W. Altmannshofer, S. Gori, J. Martín-Albo, A. Sousa and M. Wallbank, *Neutrino tridents at DUNE*, *Phys. Rev. D* **100** (2019) 115029 [arXiv:1902.06765] [INSPIRE].

[79] H. Banerjee and S. Roy, *Signatures of supersymmetry and $L_\mu - L_\tau$ gauge bosons at Belle-II*, *Phys. Rev. D* **99** (2019) 035035 [arXiv:1811.00407] [INSPIRE].

[80] D.G. Cerdeño, M. Fairbairn, T. Jubb, P.A.N. Machado, A.C. Vincent and C. Bœhm, *Physics from solar neutrinos in dark matter direct detection experiments*, *JHEP* **05** (2016) 118 [*Erratum ibid.* **09** (2016) 048] [arXiv:1604.01025] [INSPIRE].

[81] Y. Farzan, M. Lindner, W. Rodejohann and X.-J. Xu, *Probing neutrino coupling to a light scalar with coherent neutrino scattering*, *JHEP* **05** (2018) 066 [arXiv:1802.05171] [INSPIRE].

[82] D. Aristizabal Sierra, B. Dutta, S. Liao and L.E. Strigari, *Coherent elastic neutrino-nucleus scattering in multi-ton scale dark matter experiments: classification of vector and scalar interactions new physics signals*, *JHEP* **12** (2019) 124 [arXiv:1910.12437] [INSPIRE].

[83] COHERENT collaboration, *Measurement of scintillation response of CsI[Na] to low-energy nuclear recoils by COHERENT*, arXiv:2111.02477 [INSPIRE].

[84] S. Baker and R.D. Cousins, *Clarification of the use of chi square and likelihood functions in fits to histograms*, *Nucl. Instrum. Meth.* **221** (1984) 437 [INSPIRE].

[85] Particle Data Group collaboration, *Review of particle physics*, *PTEP* **2020** (2020) 083C01 [INSPIRE].

[86] A. Drukier and L. Stodolsky, *Principles and applications of a neutral current detector for neutrino physics and astronomy*, *Phys. Rev. D* **30** (1984) 2295 [INSPIRE].

[87] J. Barranco, O.G. Miranda and T.I. Rashba, *Probing new physics with coherent neutrino scattering off nuclei*, *JHEP* **12** (2005) 021 [hep-ph/0508299] [INSPIRE].

[88] K. Patton, J. Engel, G.C. McLaughlin and N. Schunck, *Neutrino-nucleus coherent scattering as a probe of neutron density distributions*, *Phys. Rev. C* **86** (2012) 024612 [arXiv:1207.0693] [INSPIRE].

[89] J. Erler and S. Su, *The weak neutral current*, *Prog. Part. Nucl. Phys.* **71** (2013) 119 [arXiv:1303.5522] [INSPIRE].

[90] O. Tomalak, P. Machado, V. Pandey and R. Plestid, *Flavor-dependent radiative corrections in coherent elastic neutrino-nucleus scattering*, *JHEP* **02** (2021) 097 [arXiv:2011.05960] [INSPIRE].

[91] A. Crivellin, M. Hoferichter, M. Kirk, C.A. Manzari and L. Schnell, *First-generation new physics in simplified models: from low-energy parity violation to the LHC*, *JHEP* **10** (2021) 221 [arXiv:2107.13569] [INSPIRE].

[92] R.H. Helm, *Inelastic and elastic scattering of* 187 *MeV electrons from selected even-even nuclei*, *Phys. Rev.* **104** (1956) 1466 [INSPIRE].

[93] J. Piekarewicz, A.R. Linero, P. Giuliani and E. Chicken, *Power of two: assessing the impact of a second measurement of the weak-charge form factor of ^{208}Pb*, *Phys. Rev. C* **94** (2016) 034316 [arXiv:1604.07799] [INSPIRE].

JHEP05(2022)109

[94] S. Klein and J. Nystrand, *Exclusive vector meson production in relativistic heavy ion collisions*, *Phys. Rev. C* **60** (1999) 014903 [hep-ph/9902259] [INSPIRE].

[95] G. Fricke et al., *Nuclear ground state charge radii from electromagnetic interactions*, *Atom. Data Nucl. Data Tabl.* **60** (1995) 177 [INSPIRE].

[96] I. Angeli and K.P. Marinova, *Table of experimental nuclear ground state charge radii: an update*, *Atom. Data Nucl. Data Tabl.* **99** (2013) 69 [INSPIRE].

[97] X.-R. Huang and L.-W. Chen, *Neutron skin in CsI and low-energy effective weak mixing angle from COHERENT data*, *Phys. Rev. D* **100** (2019) 071301 [arXiv:1902.07625] [INSPIRE].

[98] M. Hoferichter, J. Menéndez and A. Schwenk, *Coherent elastic neutrino-nucleus scattering: EFT analysis and nuclear responses*, *Phys. Rev. D* **102** (2020) 074018 [arXiv:2007.08529] [INSPIRE].

[99] D.K. Papoulias, R. Sahu, T.S. Kosmas, V.K.B. Kota and B. Nayak, *Novel neutrino-floor and dark matter searches with deformed shell model calculations*, *Adv. High Energy Phys.* **2018** (2018) 6031362 [arXiv:1804.11319] [INSPIRE].

[100] D.K. Papoulias, T.S. Kosmas and Y. Kuno, *Recent probes of standard and non-standard neutrino physics with nuclei*, *Front. in Phys.* **7** (2019) 191 [arXiv:1911.00916] [INSPIRE].

[101] E. Bertuzzo, F.F. Deppisch, S. Kulkarni, Y.F. Perez Gonzalez and R. Zukanovich Funchal, *Dark matter and exotic neutrino interactions in direct detection searches*, *JHEP* **04** (2017) 073 [arXiv:1701.07443] [INSPIRE].

[102] T. Han, J. Liao, H. Liu and D. Marfatia, *Nonstandard neutrino interactions at COHERENT, DUNE, T2HK and LHC*, *JHEP* **11** (2019) 028 [arXiv:1910.03272] [INSPIRE].

[103] L.J. Flores, N. Nath and E. Peinado, *Non-standard neutrino interactions in* $\mathrm{U}(1)'$ *model after COHERENT data*, *JHEP* **06** (2020) 045 [arXiv:2002.12342] [INSPIRE].

[104] L.M.G. de la Vega, L.J. Flores, N. Nath and E. Peinado, *Complementarity between dark matter direct searches and CEνNS experiments in* $\mathrm{U}(1)'$ *models*, *JHEP* **09** (2021) 146 [arXiv:2107.04037] [INSPIRE].

[105] CONUS collaboration, *Novel constraints on neutrino physics beyond the standard model from the CONUS experiment*, arXiv:2110.02174 [INSPIRE].

[106] M. Bauer, P. Foldenauer and J. Jaeckel, *Hunting all the hidden photons*, *JHEP* **07** (2018) 094 [arXiv:1803.05466] [INSPIRE].

[107] M. Bauer, P. Foldenauer and M. Mosny, *Flavor structure of anomaly-free hidden photon models*, *Phys. Rev. D* **103** (2021) 075024 [arXiv:2011.12973] [INSPIRE].

[108] D.W.P.d. Amaral, D.G. Cerdeno, P. Foldenauer and E. Reid, *Solar neutrino probes of the muon anomalous magnetic moment in the gauged* $\mathrm{U}(1)_{L_\mu - L_\tau}$, *JHEP* **12** (2020) 155 [arXiv:2006.11225] [INSPIRE].

[109] B.C. Allanach, J. Davighi and S. Melville, *An anomaly-free ATLAS: charting the space of flavour-dependent gauged* U(1) *extensions of the Standard Model*, *JHEP* **02** (2019) 082 [*Erratum ibid.* **08** (2019) 064] [arXiv:1812.04602] [INSPIRE].

[110] C. Giunti and C.W. Kim, *Fundamentals of neutrino physics and astrophysics*, Oxford University Press, Oxford, U.K. (2007).

JHEP05(2022)109

[111] H.-S. Lee and E. Ma, *Gauged $B - x_i L$ origin of R parity and its implications*, *Phys. Lett. B* **688** (2010) 319 [arXiv:1001.0768] [INSPIRE].

[112] T. Araki, J. Heeck and J. Kubo, *Vanishing minors in the neutrino mass matrix from Abelian gauge symmetries*, *JHEP* **07** (2012) 083 [arXiv:1203.4951] [INSPIRE].

[113] P. Coloma, M.C. Gonzalez-Garcia and M. Maltoni, *Neutrino oscillation constraints on U(1)′ models: from non-standard interactions to long-range forces*, *JHEP* **01** (2021) 114 [arXiv:2009.14220] [INSPIRE].

[114] Y. Farzan, *A model for large non-standard interactions of neutrinos leading to the LMA-dark solution*, *Phys. Lett. B* **748** (2015) 311 [arXiv:1505.06906] [INSPIRE].

[115] J. Heeck, M. Lindner, W. Rodejohann and S. Vogl, *Non-standard neutrino interactions and neutral gauge bosons*, *SciPost Phys.* **6** (2019) 038 [arXiv:1812.04067] [INSPIRE].

[116] X.-G. He, G.C. Joshi, H. Lew and R.R. Volkas, *Simplest Z' model*, *Phys. Rev. D* **44** (1991) 2118 [INSPIRE].

[117] S. Gninenko and D. Gorbunov, *Refining constraints from Borexino measurements on a light Z'-boson coupled to $L_\mu - L_\tau$ current*, *Phys. Lett. B* **823** (2021) 136739 [arXiv:2007.16098] [INSPIRE].

[118] M. Hoferichter, J. Ruiz de Elvira, B. Kubis and U.-G. Meißner, *High-precision determination of the pion-nucleon σ term from Roy-Steiner equations*, *Phys. Rev. Lett.* **115** (2015) 092301 [arXiv:1506.04142] [INSPIRE].

[119] S. Dürr et al., *Lattice computation of the nucleon scalar quark contents at the physical point*, *Phys. Rev. Lett.* **116** (2016) 172001 [arXiv:1510.08013] [INSPIRE].

[120] J. Ellis, N. Nagata and K.A. Olive, *Uncertainties in WIMP dark matter scattering revisited*, *Eur. Phys. J. C* **78** (2018) 569 [arXiv:1805.09795] [INSPIRE].

[121] C. Alexandrou et al., *Nucleon axial, tensor, and scalar charges and σ-terms in lattice QCD*, *Phys. Rev. D* **102** (2020) 054517 [arXiv:1909.00485] [INSPIRE].

[122] J.M. Alarcón, *Brief history of the pion-nucleon sigma term*, *Eur. Phys. J. ST* **230** (2021) 1609 [arXiv:2205.01108] [INSPIRE].

[123] J. Ruiz de Elvira, M. Hoferichter, B. Kubis and U.-G. Meißner, *Extracting the σ-term from low-energy pion-nucleon scattering*, *J. Phys. G* **45** (2018) 024001 [arXiv:1706.01465] [INSPIRE].

[124] E. Friedman and A. Gal, *The pion-nucleon σ term from pionic atoms*, *Phys. Lett. B* **792** (2019) 340 [arXiv:1901.03130] [INSPIRE].

[125] A. Crivellin, M. Hoferichter and M. Procura, *Accurate evaluation of hadronic uncertainties in spin-independent WIMP-nucleon scattering: disentangling two- and three-flavor effects*, *Phys. Rev. D* **89** (2014) 054021 [arXiv:1312.4951] [INSPIRE].

[126] A.M. Suliga and I. Tamborra, *Astrophysical constraints on nonstandard coherent neutrino-nucleus scattering*, *Phys. Rev. D* **103** (2021) 083002 [arXiv:2010.14545] [INSPIRE].

[127] M. Cirelli, E. Del Nobile and P. Panci, *Tools for model-independent bounds in direct dark matter searches*, *JCAP* **10** (2013) 019 [arXiv:1307.5955] [INSPIRE].

[128] P. Ilten, Y. Soreq, M. Williams and W. Xue, *Serendipity in dark photon searches*, *JHEP* **06** (2018) 004 [arXiv:1801.04847] [INSPIRE].

JHEP05(2022)109

[129] E.M. Riordan et al., *A search for short lived axions in an electron beam dump experiment*, *Phys. Rev. Lett.* **59** (1987) 755 [INSPIRE].

[130] J.D. Bjorken et al., *Search for neutral metastable penetrating particles produced in the SLAC beam dump*, *Phys. Rev. D* **38** (1988) 3375 [INSPIRE].

[131] A. Bross, M. Crisler, S.H. Pordes, J. Volk, S. Errede and J. Wrbanek, *A search for shortlived particles produced in an electron beam dump*, *Phys. Rev. Lett.* **67** (1991) 2942 [INSPIRE].

[132] A. Konaka et al., *Search for neutral particles in electron beam dump experiment*, *Phys. Rev. Lett.* **57** (1986) 659 [INSPIRE].

[133] M. Davier and H. Nguyen Ngoc, *An unambiguous search for a light Higgs boson*, *Phys. Lett. B* **229** (1989) 150 [INSPIRE].

[134] J.D. Bjorken, R. Essig, P. Schuster and N. Toro, *New fixed-target experiments to search for dark gauge forces*, *Phys. Rev. D* **80** (2009) 075018 [arXiv:0906.0580] [INSPIRE].

[135] S. Andreas, C. Niebuhr and A. Ringwald, *New limits on hidden photons from past electron beam dumps*, *Phys. Rev. D* **86** (2012) 095019 [arXiv:1209.6083] [INSPIRE].

[136] J. Blumlein et al., *Limits on neutral light scalar and pseudoscalar particles in a proton beam dump experiment*, *Z. Phys. C* **51** (1991) 341 [INSPIRE].

[137] J. Blumlein et al., *Limits on the mass of light (pseudo)scalar particles from Bethe-Heitler e^+e^- and $\mu^+\mu^-$ pair production in a proton-iron beam dump experiment*, *Int. J. Mod. Phys. A* **7** (1992) 3835 [INSPIRE].

[138] J. Blumlein and J. Brunner, *New exclusion limits for dark gauge forces from beam-dump data*, *Phys. Lett. B* **701** (2011) 155 [arXiv:1104.2747] [INSPIRE].

[139] J. Blümlein and J. Brunner, *New exclusion limits on dark gauge forces from proton bremsstrahlung in beam-dump data*, *Phys. Lett. B* **731** (2014) 320 [arXiv:1311.3870] [INSPIRE].

[140] CHARM collaboration, *Search for axion like particle production in 400 GeV proton-copper interactions*, *Phys. Lett. B* **157** (1985) 458 [INSPIRE].

[141] S.N. Gninenko, *Constraints on sub-GeV hidden sector gauge bosons from a search for heavy neutrino decays*, *Phys. Lett. B* **713** (2012) 244 [arXiv:1204.3583] [INSPIRE].

[142] NOMAD collaboration, *Search for heavy neutrinos mixing with tau neutrinos*, *Phys. Lett. B* **506** (2001) 27 [hep-ex/0101041] [INSPIRE].

[143] G. Bernardi et al., *Search for neutrino decay*, *Phys. Lett. B* **166** (1986) 479 [INSPIRE].

[144] S.N. Gninenko, *Stringent limits on the $\pi^0 \to \gamma X$, $X \to e^+e^-$ decay from neutrino experiments and constraints on new light gauge bosons*, *Phys. Rev. D* **85** (2012) 055027 [arXiv:1112.5438] [INSPIRE].

[145] H. Merkel et al., *Search at the Mainz microtron for light massive gauge bosons relevant for the muon $g-2$ anomaly*, *Phys. Rev. Lett.* **112** (2014) 221802 [arXiv:1404.5502] [INSPIRE].

[146] APEX collaboration, *Search for a new gauge boson in electron-nucleus fixed-target scattering by the APEX experiment*, *Phys. Rev. Lett.* **107** (2011) 191804 [arXiv:1108.2750] [INSPIRE].

[147] BABAR collaboration, *Search for a dark photon in e^+e^- collisions at BaBar*, *Phys. Rev. Lett.* **113** (2014) 201801 [arXiv:1406.2980] [INSPIRE].

JHEP05(2022)109

[148] KLOE-2 collaboration, *Search for a vector gauge boson in ϕ meson decays with the KLOE detector*, *Phys. Lett. B* **706** (2012) 251 [arXiv:1110.0411] [INSPIRE].

[149] KLOE-2 collaboration, *Limit on the production of a new vector boson in $e^+e^- \to U\gamma$, $U \to \pi^+\pi^-$ with the KLOE experiment*, *Phys. Lett. B* **757** (2016) 356 [arXiv:1603.06086] [INSPIRE].

[150] LHCb collaboration, *Search for dark photons produced in 13 TeV pp collisions*, *Phys. Rev. Lett.* **120** (2018) 061801 [arXiv:1710.02867] [INSPIRE].

[151] NA48/2 collaboration, *Search for the dark photon in π^0 decays*, *Phys. Lett. B* **746** (2015) 178 [arXiv:1504.00607] [INSPIRE].

[152] NA64 collaboration, *Improved limits on a hypothetical $X(16.7)$ boson and a dark photon decaying into e^+e^- pairs*, *Phys. Rev. D* **101** (2020) 071101 [arXiv:1912.11389] [INSPIRE].

[153] BABAR collaboration, *Search for invisible decays of a dark photon produced in e^+e^- collisions at BaBar*, *Phys. Rev. Lett.* **119** (2017) 131804 [arXiv:1702.03327] [INSPIRE].

[154] CONNIE collaboration, *Search for light mediators in the low-energy data of the CONNIE reactor neutrino experiment*, *JHEP* **04** (2020) 054 [arXiv:1910.04951] [INSPIRE].

[155] D. Hanneke, S. Fogwell and G. Gabrielse, *New measurement of the electron magnetic moment and the fine structure constant*, *Phys. Rev. Lett.* **100** (2008) 120801 [arXiv:0801.1134] [INSPIRE].

[156] D. Hanneke, S.F. Hoogerheide and G. Gabrielse, *Cavity control of a single-electron quantum cyclotron: measuring the electron magnetic moment*, *Phys. Rev. A* **83** (2011) 052122 [arXiv:1009.4831] [INSPIRE].

[157] L. Morel, Z. Yao, P. Cladé and S. Guellati-Khélifa, *Determination of the fine-structure constant with an accuracy of 81 parts per trillion*, *Nature* **588** (2020) 61 [INSPIRE].

[158] CMS collaboration, *Search for an $L_\mu - L_\tau$ gauge boson using $Z \to 4\mu$ events in proton-proton collisions at $\sqrt{s} = 13$ TeV*, *Phys. Lett. B* **792** (2019) 345 [arXiv:1808.03684] [INSPIRE].

[159] BABAR collaboration, *Search for a muonic dark force at BABAR*, *Phys. Rev. D* **94** (2016) 011102 [arXiv:1606.03501] [INSPIRE].

[160] CCFR collaboration, *Neutrino tridents and WZ interference*, *Phys. Rev. Lett.* **66** (1991) 3117 [INSPIRE].

[161] W. Altmannshofer, S. Gori, M. Pospelov and I. Yavin, *Neutrino trident production: a powerful probe of new physics with neutrino beams*, *Phys. Rev. Lett.* **113** (2014) 091801 [arXiv:1406.2332] [INSPIRE].

[162] G. Bellini et al., *Precision measurement of the ^{7}Be solar neutrino interaction rate in Borexino*, *Phys. Rev. Lett.* **107** (2011) 141302 [arXiv:1104.1816] [INSPIRE].

[163] A. Kamada and H.-B. Yu, *Coherent propagation of PeV neutrinos and the dip in the neutrino spectrum at IceCube*, *Phys. Rev. D* **92** (2015) 113004 [arXiv:1504.00711] [INSPIRE].

[164] R. Barbieri and T.E.O. Ericson, *Evidence against the existence of a low mass scalar boson from neutron-nucleus scattering*, *Phys. Lett. B* **57** (1975) 270 [INSPIRE].

[165] J. Schmiedmayer, H. Rauch and P. Riehs, *Measurement of the electric polarizability of the neutron*, *Phys. Rev. Lett.* **61** (1988) 1065 [INSPIRE].

JHEP05(2022)109

[166] H. Leeb and J. Schmiedmayer, *Constraint on hypothetical light interacting bosons from low-energy neutron experiments*, *Phys. Rev. Lett.* **68** (1992) 1472 [INSPIRE].

[167] J.M. Berryman, A. De Gouvêa, K.J. Kelly and Y. Zhang, *Lepton-number-charged scalars and neutrino beamstrahlung*, *Phys. Rev. D* **97** (2018) 075030 [arXiv:1802.00009] [INSPIRE].

[168] M.S. Bilenky and A. Santamaria, *'Secret' neutrino interactions*, in *Neutrino mixing: meeting in honor of Samoil Bilenky's* 70^{th} *birthday*, (1999), p. 50 [hep-ph/9908272] [INSPIRE].

[169] A.P. Lessa and O.L.G. Peres, *Revising limits on neutrino-Majoron couplings*, *Phys. Rev. D* **75** (2007) 094001 [hep-ph/0701068] [INSPIRE].

[170] P.S. Pasquini and O.L.G. Peres, *Bounds on neutrino-scalar Yukawa coupling*, *Phys. Rev. D* **93** (2016) 053007 [*Erratum ibid.* **93** (2016) 079902] [arXiv:1511.01811] [INSPIRE].

[171] G. Krnjaic, G. Marques-Tavares, D. Redigolo and K. Tobioka, *Probing muonphilic force carriers and dark matter at kaon factories*, *Phys. Rev. Lett.* **124** (2020) 041802 [arXiv:1902.07715] [INSPIRE].

[172] V. Brdar, M. Lindner, S. Vogl and X.-J. Xu, *Revisiting neutrino self-interaction constraints from Z and τ decays*, *Phys. Rev. D* **101** (2020) 115001 [arXiv:2003.05339] [INSPIRE].

[173] M. Agostini et al., *Results on $\beta\beta$ decay with emission of two neutrinos or Majorons in ^{76}Ge from GERDA phase I*, *Eur. Phys. J. C* **75** (2015) 416 [arXiv:1501.02345] [INSPIRE].

[174] KamLAND-Zen collaboration, *Limits on Majoron-emitting double-beta decays of ^{136}Xe in the KamLAND-Zen experiment*, *Phys. Rev. C* **86** (2012) 021601 [arXiv:1205.6372] [INSPIRE].

[175] K. Blum, Y. Nir and M. Shavit, *Neutrinoless double-beta decay with massive scalar emission*, *Phys. Lett. B* **785** (2018) 354 [arXiv:1802.08019] [INSPIRE].

[176] A. Keshavarzi, K.S. Khaw and T. Yoshioka, *Muon $g-2$: a review*, *Nucl. Phys. B* **975** (2022) 115675 [arXiv:2106.06723] [INSPIRE].

[177] S. Li, Y. Xiao and J.M. Yang, *A pedagogical review on muon $g-2$*, *Physics* **4** (2021) 40 [arXiv:2110.04673] [INSPIRE].

[178] S.J. Brodsky and E. De Rafael, *Suggested boson-lepton pair couplings and the anomalous magnetic moment of the muon*, *Phys. Rev.* **168** (1968) 1620 [INSPIRE].

JHEP05(2022)109